Check for updates

Geochemistry, Geophysics, Geosystems®

AGU ADVANCING EARTH AND SPACE SCIENCE

RESEARCH ARTICLE
10.1029/2022GC010843

Special Section:
Africa plate geosystems

The Atlas of Morocco: A Plume-Assisted Orogeny

R. Lanari[1,2], C. Faccenna[2,3], C. Natali[1,4], E. Şengül Uluocak[5], M. G. Fellin[6], T. W. Becker[7,8,9], O. H. Göğüş[10], N. Youbi[11,12], R. Clementucci[2,6,13], and S. Conticelli[1,4]

[1]Department of Earth Sciences, University of Florence, Florence, Italy, [2]Department of Science, RomaTre University, Rome, Italy, [3]GFZ, German Research Center for Geoscience, Potsdam, Germany, [4]CNR, Institute of Environmental Geology and Geoengineering, Montelibretti, Italy, [5]Faculty of Engineering, Geophysics, Canakkale Onsekiz Mart University, Canakkale, Turkey, [6]Department of Earth Sciences, ETH Zurich, Zurich, Switzerland, [7]Institute for Geophysics, The University of Texas at Austin, Austin, TX, USA, [8]Department of Geological Sciences, The University of Texas at Austin, Austin, TX, USA, [9]Oden Institute for Computational Engineering and Sciences, The University of Texas at Austin, Austin, TX, USA, [10]Eurasia Institute of Earth Sciences, Istanbul Technical University, Istanbul, Turkey, [11]Department of Geology, Faculty of Sciences-Semlalia, Cadi Ayyad University, Marrakesh, Morocco, [12]Faculty of Geology and Geography, Tomsk State University, Tomsk, Russia, [13]CNRS, IRD, INRAE, Collège de France, CEREGE, Aix-Marseille University, Aix-en Provence, France

Abstract We explore the connections between crustal shortening, volcanism, and mantle dynamics in the Atlas of Morocco. In response to compressional forces and strain localization, this intraplate orogen has evolved far from convergent plate margins. Convective effects, such as lithospheric weakening and plume-related volcanism, contributed in important ways to the building of high topography. We seek to better understand how crustal and mantle processes interacted during the Atlas' orogeny by combining multiple strands of observations, including new and published data. Constraints on crustal and thermal evolution are combined with new analyses of topographic evolution, petrological, and geochemical data from the Anti-Atlas volcanic fields, and a simple numerical model of the interactions among crustal deformation, a mantle plume, and volcanism. Our findings substantiate that: (a) crustal deformation and exhumation accelerated during the middle/late Miocene, contemporaneous with the onset of volcanism; (b) volcanism has an anorogenic signature with a deep source; (c) a dynamic mantle upwelling supports the high topography. We propose that a mantle plume and the related volcanism weakened the lithosphere beneath the Atlas and that this favored the localization of crustal shortening along pre-existing structures during plate convergence. This convective-tectonic sequence may represent a general mechanism for the modification of continental plates throughout the thermo-chemical evolution of the supercontinental cycle.

Key Points:

- Crustal thickening is limited and cannot account for the topography elevation of the Atlas system
- Resumption of volcanism is contemporaneous with the acceleration of crustal deformation and topography growing
- The erosion and weakening of the lower lithosphere, as a consequence of mantle plume, may enhance crustal deformation and exhumation

Supporting Information:

Supporting Information may be found in the online version of this article.

Correspondence to:

R. Lanari,
riccardo.lanari@uniroma3.it

Citation:

Lanari, R., Faccenna, C., Natali, C., Şengül Uluocak, E., Fellin, M. G., Becker, T. W., et al. (2023). The Atlas of Morocco: A plume-assisted orogeny. *Geochemistry, Geophysics, Geosystems*, *24*, e2022GC010843. https://doi.org/10.1029/2022GC010843

Received 3 JAN 2023
Accepted 8 MAY 2023

© 2023. The Authors. Geochemistry, Geophysics, Geosystems published by Wiley Periodicals LLC on behalf of American Geophysical Union.
This is an open access article under the terms of the Creative Commons Attribution-NonCommercial-NoDerivs License, which permits use and distribution in any medium, provided the original work is properly cited, the use is non-commercial and no modifications or adaptations are made.

1. Introduction

Orogenic belts form primarily at convergent margins when the velocity of subduction is slower than the velocity of convergence (e.g., Faccenna et al., 2021). This may be due to a decrease in the buoyancy of the subducting slab, for example, related to the arrival at the trench of continental lithosphere or an oceanic plateau (e.g., Cloos & Shreve, 1988; Royden & Faccenna, 2018), or due to a stalling of the trench (Faccenna et al., 2017; Russo & Silver, 1996). However, some orogenic belts form far away from convergent margins. This is usually associated with the propagation of compressional stress for some hundreds of kilometers from the margin. This may be induced by flat subduction, which causes a broadening of the deformed zone, as in the Laramide-Western Cordillera of the Andes (DeCelles et al., 2014; Isacks et al., 1968). Alternatively, intraplate compression can also be caused by the transformation of a nearby convergent margin into a hard-collisional one, for example, for the Pyrenees, Caucasus, Alborz, Kopet Dagh, and Tien Shan (Ballato et al., 2011). In any case, shortening localizes along pre-existing zones of weakness, likely where the lithospheric mantle is removed, causing a significant strength drop. This may be due to a prior extensional phase, provided that the time lag between the two deformational phases is short enough to avoid thermal resetting to other mantle processes or both.

Formation of intracontinental orogenic belts may then provide information about intraplate stress propagation (i.e., plate tectonic forcing), strain localization processes and lithospheric weakening due to mantle dynamics (i.e., lithospheric removal, plume-like upwelling). Disentangling the interplay of those processes is complicated by crustal structural heterogeneities and different spatial wavelengths and timescales at which these processes

15252027, 2023, 6, Downloaded from https://agupubs.onlinelibrary.wiley.com/doi/10.1029/2022GC010843 by Thorsten Becker - University Of Texas Libraries , Wiley Online Library on [12/06/2023]. See the Terms and Conditions (https://onlinelibrary.wiley.com/terms-and-conditions) on Wiley Online Library for rules of use; OA articles are governed by the applicable Creative Commons License

occur. However, three processes are fundamental to capture the dynamics of intracontinental orogeny: (a) crustal deformation, (b) topography evolution, and (c) thermal evolution and magmatism.

Here, we discuss the case of the High-, Middle Atlas and Anti Atlas of Morocco as a natural laboratory, a well-documented site to understand the potential feedback between mantle dynamics and crustal deformation. The current Atlas setting shows evidence of dynamic surface uplift (Babault et al., 2008; Faccenna & Becker, 2020; Miller & Becker, 2014; Miller et al., 2015; Missenard & Cadoux, 2012; Teixell et al., 2005), volcanism (Berger et al., 2008; Berger, Ennih, et al., 2009; Berger, Liégeois, et al., 2009; Duggen et al., 2009), and crustal deformation (Ellero et al., 2012; Lanari et al., 2020a; Missenard et al., 2007) primarily occurring since Neogene.

Different models have been proposed for the origin of the high topography and volcanism, suggesting a mantle upwelling related to the Canary plume, which originates ∼1,000 km southwest of the Atlas system (Civiero et al., 2018; Duggen et al., 2009), lithospheric thinning by delamination-peel back lithosphere, viscous dripping, plume-like mantle upwelling (Missenard et al., 2006; Ramdani, 1998; Zeyen et al., 2005), or edge driven convection (Missenard & Cadoux, 2012), but the linkage between crustal shortening (including inherited structures), volcanism, and lithospheric thinning/mantle upwelling, and their timing has not been hitherto addressed.

The aim of this paper is to explore the connections between the Miocene crustal shortening, volcanism, and mantle dynamics in the Atlas. We discuss three sets of observations that are derived by integrating previous data with new analyses and inferences. First, we analyze the main geologic constraints of crustal and thermal evolution of the belt using three cross sections. Second, we analyze the topography at different wavelengths using admittance analysis, and estimating the residual topography. Third, we present new petrology and geochemistry data together with new ages on the Anti Atlas (Siroua and Saghro) volcanic fields. Petrological interpretations are also placed into a broader context, at the scale of the whole Atlas system, to better constrain the Miocene period of Moroccan volcanism (Figure 1).

From those three data sets, we infer that: (a) crustal deformation and exhumation accelerated during the middle/late Miocene, contemporaneous with the resumption of volcanism; (b) volcanism has an anorogenic signature with a deep source; (c) a dynamic deep mantle source supported the high topography. Volcanism, uplift, and crustal deformation occurred contemporaneously from the late Miocene onward. Lastly, we conducted simple numerical tests to investigate the connections between mantle dynamics and crustal deformation. Such models are geared toward a better understanding of general processes rather than perfectly replicating the details and specific history of the Atlas system. These efforts and our results lead us to propose a new model, where a mantle upwelling and related volcanism weaken the lithosphere and favor crustal shortening, that is localized along pre-existing structural fabrics due to plate convergence (e.g., Lanari et al., 2020a, 2020b; Skikra et al., 2021).

2. Tectonic, Volcanism, Topography and Deep Structure in the High and Anti Atlas

2.1. Tectonic and Exhumation

The High Atlas trends WSW-ENE for 650 km and can be subdivided into Western, Central and Eastern High Atlases. The Western and Central High Atlas topography rises to 4 and 3.5 km, respectively. The Anti Atlas extends with the same trend for ∼400 km reaching 2.5 km of elevation (Figure 1a). The Western High Atlas and the Anti Atlas are linked by the Siroua volcanic field, which rises over 3 km in elevation (Figure 1). The overall structural setting of the High and Middle Atlas, as for all of NW Africa, is dominated by a dextral shear zone (Soumaya et al., 2018) as a consequence of the oblique tectonic transport direction (Dewey et al., 1989). Transpressional tectonics has been documented both in the Middle and High Atlases (Ellero et al., 2012; Gomez et al., 1998; Lanari et al., 2020b). Here, Cenozoic inversion reactivated several inherited structures from the Triassic-Jurassic, resulting in strain partitioning with oblique-slip faults in the inner portion and thrust-related folding in the frontal region of the belt (Delcaillau et al., 2011; Ellero et al., 2012; Lanari et al., 2020b). Along the High Atlas, despite the oblique tectonic transport direction, the degree of transpression vanishes eastward (Lanari et al., 2020b). Thus, the Central High Atlas range is structurally dominated by folding-and-thrusting faults rather than oblique-slip faults (Calvín et al., 2018; Teixell et al., 2003, 2017). In turn, this complex deformation style affects the amount of total shortening, which changes along the strike. NNW-SSE sections present shortening estimates ranging from ≈14 km (17%–20%, Domènech et al., 2016; Fekkak et al., 2018) and 12–15 km in the WHA (15%–21%, Domènech et al., 2016; Lanari et al., 2020a; Missenard et al., 2007; Teixell et al., 2003) to 30–34 km in the Central High Atlas (30%, Beauchamp et al., 1999; Gomez et al., 2000; Teixell et al., 2003).

10.1029/2022GC010843

15252027, 2023, 6, Downloaded from https://agupubs.onlinelibrary.wiley.com/doi/10.1029/2022GC010843 by Thorsten Becker - University Of Texas Libraries , Wiley Online Library on [12/06/2023]. See the Terms and Conditions (https://onlinelibrary.wiley.com/terms-and-conditions) on Wiley Online Library for rules of use; OA articles are governed by the applicable Creative Commons License

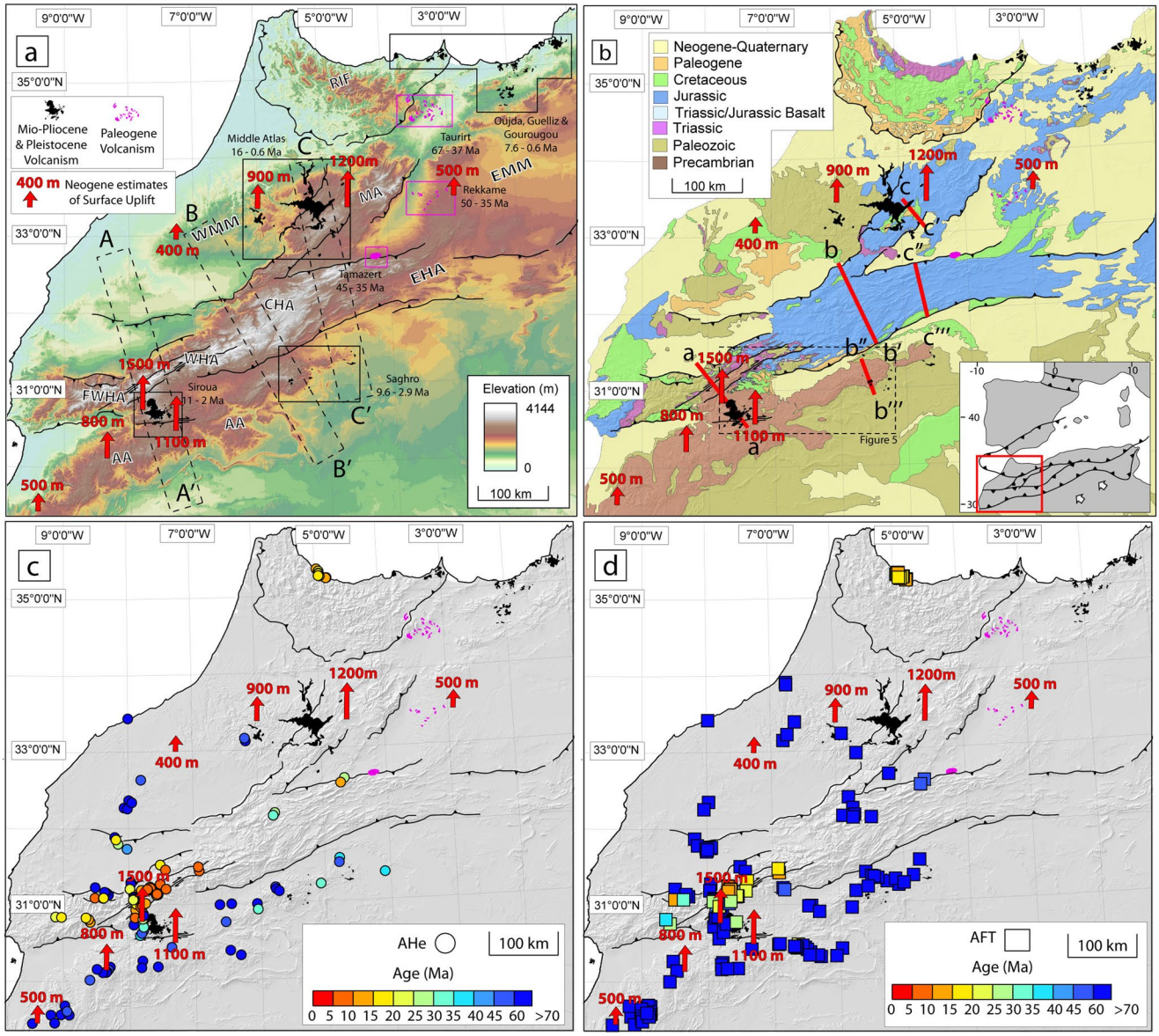

Figure 1. (a) Topographic map of North West Africa. Rectangles with dashed contours (AA', BB', CC', and DD') indicate the traces of the swath profiles shown in Figure 9. (b) Schematic geological map of the High Atlas and Anti Atlas of Morocco. Red lines (aa', bb', and cc'c") indicate the traces of the geologic section shown in Figure 2. FWHA, Far Western High Atlas; WHA, Western High Atlas; CHA, Central High Atlas; EHA, Eastern High Atlas; AA, Anti Atlas; MA, Middle Atlas; EMM, Eastern Moroccan Meseta; WMM, Western Moroccan Meseta (c, d) Apatite (U-Th)/He (AHe) cooling ages and apatite fission-track cooling ages from previous studies (see references in Lanari, Boutoux, et al., 2023).

In the WHA, the amount of shortening rises to ≈25 km when accounting for oblique-slip deformation (Lanari et al., 2020b).

In the Atlas, field geological surveys and thermochronological studies indicate that compression started during the late Eocene (Frizon de Lamotte et al., 2009; Leprêtre et al., 2015, 2018). The main surge of compression started in the middle-late Miocene (Figures 1c and 1d; Balestrieri et al., 2009; Barbero et al., 2007, 2011; Domènech, 2015; Domènech et al., 2016; Ghorbal, 2009; Ghorbal et al., 2008; Lanari et al., 2020b; Lanari, Boutoux, et al., 2023; Missenard et al., 2008) and persisted at lower rates until recent times (Arboleya et al., 2008; Tesòn & Teixell, 2008). To the north, along the Rif, cooling ages indicate a lower-middle Miocene exhumation phase (Figures 1c and 1d) (Azdimousa et al., 2014). In the High Atlas, the amount of exhumation also changes along the strike. In the WHA, apatite fission-track (AFT) and zircon (U-Th)/He ages constrain the amount of

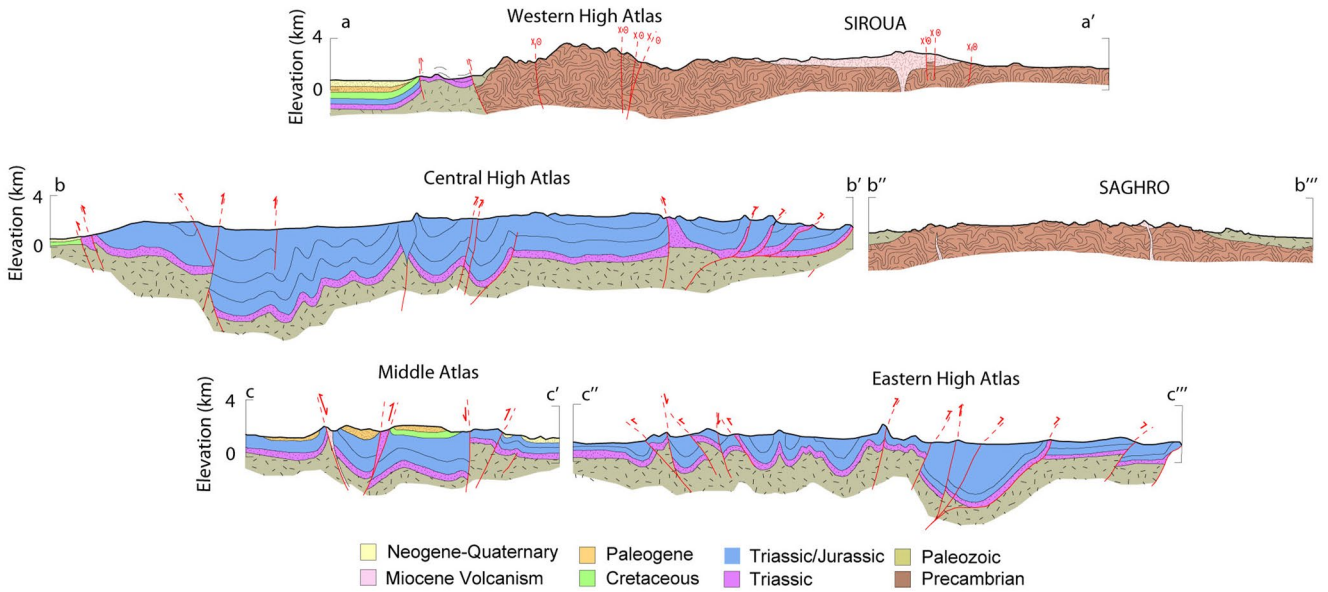

Figure 2. Geologic sections across the Western, Central, and Eastern High Atlas: the locations of the traces are shown in Figure 1b. (aa') is from Lanari et al. (2020a). (bb') and (c'c") are modified after Teixell et al. (2003). (cc') is modified after Arboleya et al. (2004). In the Western High Atlas, Cenozoic deformation occurred along steep oblique-slip faults that reactivated inherited structures across basement rocks, whereas in the Central and Eastern High Atlas, it occurred predominantly by folding and thrusting of thick Mesozoic sedimentary rocks.

exhumation to 4–6 km, whereas non-reset AFT ages in the Central High Atlas suggest that the exhumation did not exceed 3 km (Lanari et al., 2020b).

In the Anti Atlas, landform analyses based on unconformities or tilted surfaces indicate a late-Miocene uplift (Guimerà et al., 2011; Hssaine & Bridgland, 2009) that is coeval with a late Miocene volcanic event and the consequent emplacement of two volcanic fields: the Siroua in the western, and the Saghro in the eastern (Figure 1) (Berrahma et al., 1993; Guimerà et al., 2011). Overall, Miocene deformation is not documented along the Anti Atlas, with the exception of a large E-W strike slip fault cross-cutting Miocene Siroua volcanics (Lanari et al., 2020a). In the Anti Atlas, cooling ages are remarkably old, suggesting slow and limited exhumation during the Neogene (Figures 1c and 1d) (Charton et al., 2020; Gouiza et al., 2017; Lanari et al., 2020b; Malusà et al., 2007; Oukassou et al., 2013; Ruiz et al., 2011; Sebti et al., 2009). Lastly, the Quaternary evolution of the Anti Atlas is still poorly constrained compared to the WHA where morphological and seismotectonic evidence indicate uplift and deformation (e.g., Boulton et al., 2014; Meghraoui et al., 1999; Pastor et al., 2012; Sébrier et al., 2006). Volcanism ceased after 2 Ma (Berrahma et al., 1993; Delaloye, 1989) and morphological features suggest a waning of uplift since ~2 Ma (Lanari et al., 2022).

2.2. Volcanism

Jurassic, Paleogene, and Neogene/Pleistocene volcanism is widespread all-over northwestern Africa and southern Spain (Figure 1; Casalini et al., 2022; Duggen et al., 2009; Mattei et al., 2014; Turner et al., 1999), but only the most recent events occurred concurrently with the High- and Middle-Atlas orogenic evolution. Mafic Neogene/Pleistocene volcanic products are found all along the Atlas belts and on the Mediterranean coast (e.g., Siroua, Saghro, Middle Atlas, Guilliz, Gourougou and Oujda-Oranie; Figure 1). Anti and Middle Atlas volcanics include alkaline and subalkaline rocks characterized by Sr-Nd isotopic composition that suggests a lithospheric mantle origin (Baziotis et al., 2019; Berger et al., 2014; Berrahma & Delaloye, 1989; Berrahma et al., 1993; Chanouan et al., 2017; Choubert et al., 1968; El Messbahi et al., 2015; Malarkey et al., 2011; Natali et al., 2013; Raffone et al., 2009; Soukrati et al., 2021; Wittig, Pearson, Baker, et al., 2010; Wittig, Pearson, Duggen, et al., 2010). On the other hand, alkaline lavas from the Rif (Figure 1) are characterized by lower Sr and higher Nd isotopic ratios, with respect to the Anti and Middle Atlas rocks, which are more compatible with a sub-lithospheric mantle source (Duggen et al., 2005). Overall, Moroccan volcanism is primarily related to anorogenic magmatism, especially for the Middle and Anti Atlas, whereas in the northern sector the volcanism is subduction-related with the

15252027, 2023, 6, Downloaded from https://agupubs.onlinelibrary.wiley.com/doi/10.1029/2022GC010843 by Thorsten Becker - University Of Texas Libraries , Wiley Online Library on [12/06/2023]. See the Terms and Conditions (https://onlinelibrary.wiley.com/terms-and-conditions) on Wiley Online Library for rules of use; OA articles are governed by the applicable Creative Commons License

15252027, 2023, 6, Downloaded from https://agupubs.onlinelibrary.wiley.com/doi/10.1029/2022GC010843 by Thorsten Becker - University Of Texas Libraries , Wiley Online Library on [12/06/2023]. See the Terms and Conditions (https://onlinelibrary.wiley.com/terms-and-conditions) on Wiley Online Library for rules of use; OA articles are governed by the applicable Creative Commons License

exception of a small occurrence of alkaline lavas from the Rif volcanic field with a clear anorogenic geochemical fingerprint (negative anomalies K, Zr, Hf, Ti in spider diagrams, at Guilliz, Oujida, and Gourougou; Duggen et al., 2009; El Azzouzi et al., 2014, 2010).

2.3. Topography and Deep Structure

The minimum amount of surface uplift estimates for the Anti-Atlas from uplifted relict landscape vary from 500 m to more than 1,500 m in the western to the central Anti-Atlas sectors, and 1,150 m in the Siroua Massif, indicative of uplift since the middle-late Miocene (Figure 1; Clementucci et al., 2022). The peak of uplift is found in the Siroua area where additional uplift mechanisms appear superimposed onto a longer wavelength trend. To the north, the Western Moroccan Meseta is also characterized by rejuvenated topography, with transient adjustment of hillslopes and fluvial channels to new uplift conditions. The magnitude of surface uplift increases from 400–500 to 900 m and 1,100–1,200 m from the Western Moroccan Meseta to the Middle Atlas (Clementucci et al., 2022; Pastor et al., 2015). In addition, shallow marine deposits between the Middle Atlas and the Western Moroccan Meseta indicate a shallowing-upward trend at ∼7 Ma, representing an important marker to constrain the timing of uplift in this sector (Babault et al., 2008; Clementucci et al., 2023a, 2023b; Krijgsman et al., 1999).

The High Atlas topography and uplift estimates since the late Miocene are in contrast with modest crustal thickening and limited amounts of exhumation that occurred during the same time (Lanari et al., 2020a, 2020b; Teixell et al., 2003). This suggests that contributions other than crustal isostasy are important (Babault et al., 2008; Missenard et al., 2006; Teixell et al., 2005). Seismology shows that the crust beneath the High Atlas ranges between 35 and 40 km, slightly deeper to the crustal thickness in the northern and southern areas, where it ranges between 33 and 36 km (Ayarza et al., 2005, 2014; Makris et al., 1985; Palomeras et al., 2017; Tadili et al., 1986). Receiver function analysis indicates crustal thicknesses in the WHA of 30–40 km, in the Central High Atlas of 33–40 km (Mancilla & Diaz, 2015), and in the Eastern High Atlas between 30 and 35 km (Miller & Becker, 2014; Sun et al., 2014) or up to 50 km (Miller et al., 2015). *P*-wave travel times indicate the presence of a thin and/or an extremely hot lithosphere beneath the High Atlas (Seber et al., 1996), and a hot asthenospheric anomaly underneath the Eastern High Atlas was inferred based on waveform modeling by Sun et al. (2014). Shear wave tomography for the crust and upper mantle indicates a lithospheric thickness of ∼80 km in the WHA and up to 95 km beneath the Central High Atlas (Palomeras et al., 2017). Receiver function estimates suggest a lithospheric thickness of ∼100 km (Miller & Becker, 2014; Miller et al., 2015). Thermal and density models imply 70–90 km thick lithosphere (Zeyen et al., 2005).

3. Methods and Results

3.1. Topographic Analysis

We analyze topography using; (a) admittance, (b) filtered topography, and (c) residual topography estimates.

1. We explore the correlation between observed topography (t) and free-air gravity data (g) (Bonvalot et al., 2012) as a function of wavenumber ($k = 2\pi/\lambda$) for the region shown in Figure 3a. To this end, we use a Thomson multiple-Slepian-taper spectral analysis method to obtain admittance ($Z(k)$) and coherence ($\gamma^2(k)$) functions from topography and gravity data (Simons et al., 2000; Thomson, 1982; Uluocak et al., 2016). We show the average values of the admittance ($Z(k) = S_{gt}(k)/S_t(k)$) with the standard deviations over wavenumbers, coherence ($\gamma^2(k) = S_{gt}{}^2(k)/S_g(k)/S_t(k)$) between topography and gravity is given as the average values ($\bar{\gamma}^2$) in Figure 3b. The spectral density functions (i.e., S_{gt}, S_t, and S_g) are calculated from the data, which are finite and non-periodic (i.e., t-topography and g-gravity) using the weighted average of the spectra corresponding to the selected spectral windows (Pérez-Gussinyé et al., 2007; Şengül-Uluocak et al., 2019). In this method, windows with overlapping tapers provide a way to reduce the variance of the estimates with minimal spectral leakage. Taper numbers (2NW-1) are defined from the resolution bandwidth (NW) and the physical size of the data (N are the data samples in a Δt sampling interval). We use NW = 4 and 2NW-1 = 7 (eigentaper numbers) by following the conventional approach in the multitaper method (Simons et al., 2000; Şengül-Uluocak et al., 2019). Although detailed bandwidth analyses are not the main focus here (cf. Simons et al., 2000), we note that small NW values lead to loss of information, while high values reduce the resolution in the wavenumber domain. Dynamic support of topography yields non-zero gravity admittance values at long wavelengths, whereas the increasing admittance at short wavelengths can be explained by uncompensated,

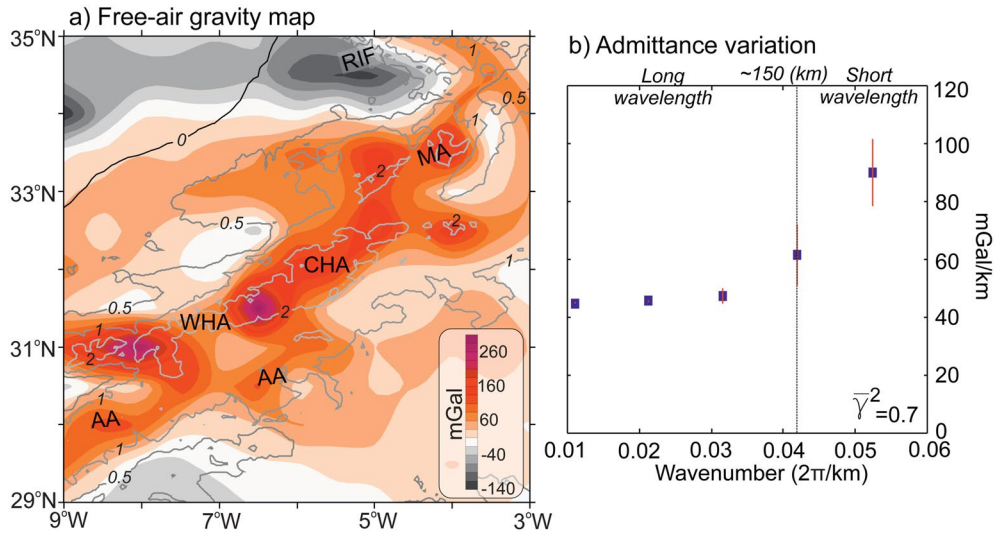

Figure 3. (a) Free-air gravity anomaly map obtained from Earth Gravitational Model-2012 (Bonvalot et al., 2012) with a 50 × 50 km gridding interval (contours show the elevation in km). (b) Average variations of admittance function with the standard deviation that is calculated for the area shown in (a). $\overline{\gamma}^2$ indicates the mean value of the coherence at all wavelengths.

flexural support (e.g., McKenzie & Fairhead, 1997; Molnar & Houseman, 2015). Accordingly, the resulting admittance with a mean value of ∼50 mGal/km at long wavelengths ($\lambda \geq 150$ km) might indicate the convective support for the topography due to the upwelling mantle beneath the region. In concordance with the good correlation between free-air gravity and topography at all wavelengths ($\overline{\gamma}^2 = \sim 0.7$), Figure 3a shows the SW-NE orientation of gravity anomalies with the high values (∼≥150 mGal) localized over the Moroccan volcanic fields (i.e., Siroua and Saghro) implying dynamic support (e.g., Craig et al., 2011).

2. In addition, to qualitatively test whether large wavelength processes are supporting the topography of the Atlas, we filtered the topography signal through a "circle average" consisting of averaging each pixel with areas with diameters of 10, 50, 100, and 150 km (Figures 4a–4d). This well-established method has been applied to several other locations (e.g., Apennines; Lanari, Reitano, et al., 2023; Carpathians; Molin et al., 2012) and qualitatively allows differentiating regional-scale features from short wavelength topographic characteristics supported by tectonic or elastic flexure (Roy et al., 2009; Wegmann et al., 2007). If the large wavelength topography matches the actual one, it is then possible to deduce that the actual topography is likely sustained by the mantle. On the other hand, if local faulting or crustal isostasy control the topographic evolution, only short wavelength-filtered topography is expected to resemble the modern one (e.g., D'Agostino et al., 2001). Overall, at long wavelengths, the high topography shows an elongated SW-NE oriented feature that peaks in the Central High Atlas. In the WHA, the high topography is shifted to the south over the Siroua volcanic field, whereas in the northern sectors, the high topography is in the southeastern part of the Middle Atlas (Figure 4a–4d).
3. Lastly, we estimate the non-isostatic component of topography (residual) from a lithospheric thickness model (Figure 4e). We use the regional crustal thickness compilation by Diaz, Gallart, and Carbonell (2016), Díaz, Gil, et al. (2016) (Figure 4f) combined with the global crustal model CRUST1.0 (Laske et al., 2013). All topography estimates have the short wavelength structure removed by convolution with a Gaussian smoothing kernel of 6σ width of 250 km. Models assume a constant lithosphere thickness of 100 km and a reference density of 2,775 and 3,250 kg/m^3 for the crust and the lithospheric mantle, respectively. For one model, we allow for lateral variations in crustal density as inferred from the column averages of CRUST1.0 (Laske et al., 2013). The asthenospheric density value is set to minimize the residual in order to attribute the maximum possible topography variations to isostasy, and best fit values range from 3,202 to 3,210 kg/m^3 (Faccenna & Becker, 2020). Overall, residual topography estimates show a positive signal over the Atlas, which is flanked by two negative anomalies in the northwestern and southwestern of Morocco: in the western Rif and in the Sahara, where the crustal structures are less constrained. The maximum positive signal is ∼850 m beneath the Central High Atlas and extends up the Middle Atlas, while the negative signal reaches almost ∼1,200 m beneath the Rif (Figure 4e).

15252027, 2023, 6, Downloaded from https://agupubs.onlinelibrary.wiley.com/doi/10.1029/2022GC010843 by Thorsten Becker - University Of Texas Libraries , Wiley Online Library on [12/06/2023]. See the Terms and Conditions (https://onlinelibrary.wiley.com/terms-and-conditions) on Wiley Online Library for rules of use; OA articles are governed by the applicable Creative Commons License

10.1029/2022GC010843

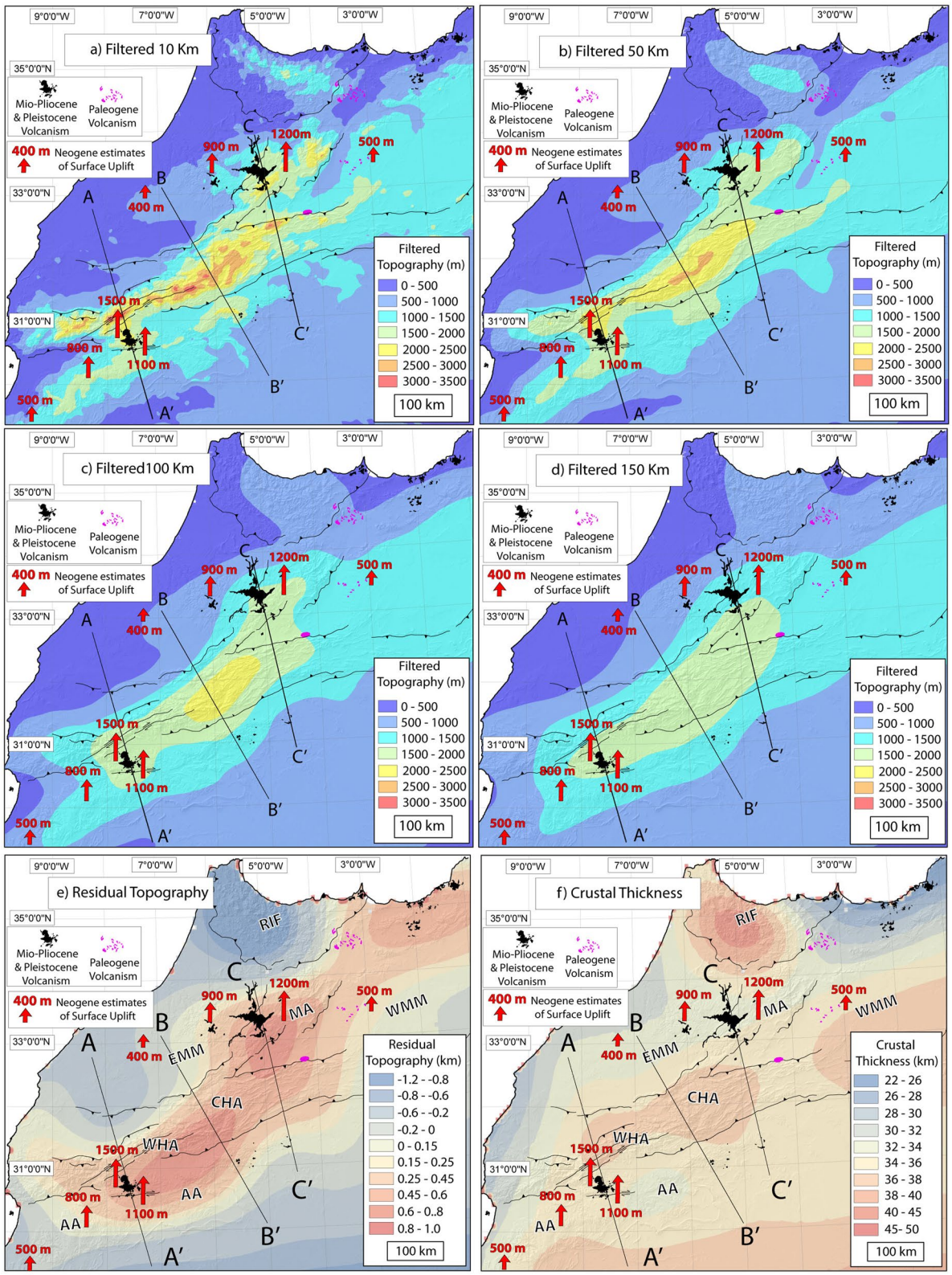

Figure 4. Filtered topography with 10 (a), 50 (b), 100 (c), and 150 (d) km average window. (e) residual topography from Civiero et al. (2020), (f) Crustal thickness form Crust1 and Díaz, Gil, et al. (2016), Black lines represent the trace of the sections. Red arrows indicate data of surface uplift from Clementucci et al. (2022).

15252027, 2023, 6, Downloaded from https://agupubs.onlinelibrary.wiley.com/doi/10.1029/2022GC010843 by Thorsten Becker - University Of Texas Libraries , Wiley Online Library on [12/06/2023]. See the Terms and Conditions (https://onlinelibrary.wiley.com/terms-and-conditions) on Wiley Online Library for rules of use; OA articles are governed by the applicable Creative Commons License

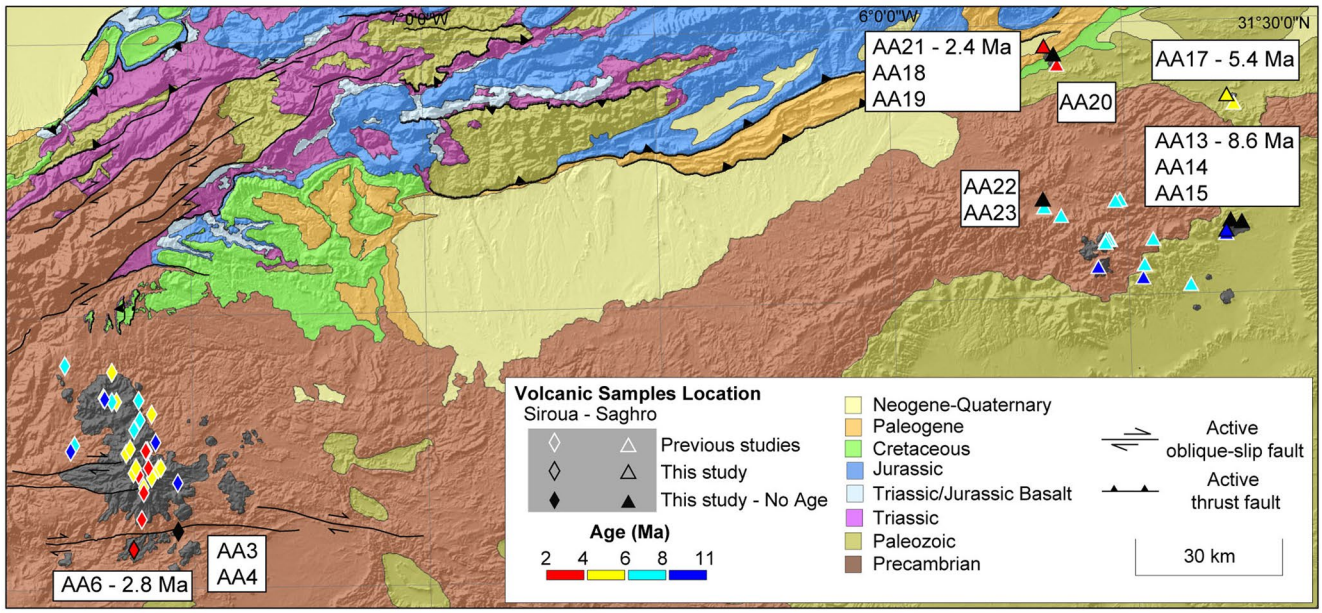

Figure 5. Detailed geological map of the central-eastern Anti Atlas with the location of previous and new samples.

3.2. Petrographic, Geochemical and Geochronological Analysis

In the Anti Atlas, Cenozoic volcanism is restricted to the Siroua and the Saghro volcanic fields, which were active from 10.8 to 2.8 Ma (Berrahma & Delaloye, 1989; Berrahma et al., 1993). We focus on these Anti Atlas volcanic fields collecting and analyzing 13 new samples (Figure 5 and Table S2), with the aim to better constrain the age and affinity of the volcanism and its geodynamic significance.

The Siroua volcanic field is characterized by the occurrence of a well-developed strato-volcano, placed in the Northern portion of the volcanic field, associated with several monogenetic volcanoes mainly aligned along an East-West trend according to the main regional faults (Berrahma & Hernandez, 1985). The volcanic rocks emplaced through three pulses of volcanism (Berrahma & Delaloye, 1989). Pyroclastic rocks were dominated by lava flows in the main stratovolcano, whereas scoria cones and small linear lava flows dominated the monogenetic apparata of the southern sector (e.g., Berrahma & Delaloye, 1989; Bondi et al., 2002).

The Saghro volcanic field is characterized by the occurrence of several monogenetic volcanic apparata and domes arranged along two East-West alignments emplaced, analogously to Siroua, through three pulses of volcanism with volcanic products emplaced between 9.6 and 2.9 Ma (Berrahma et al., 1993).

On the collected samples, petrographic features, major and trace element compositions, Sr-Nd-Pb isotopic ratios, and new geochronologic ages were determined and then described below and summarized in Tables S2 and S3.

The four new K/Ar ages determined on mafic lavas yield ages between 8.6 and 2.4 Ma (Table S3) falling well within the range of ages found for Siroua and Saghro volcanic fields (Berrahma & Delaloye, 1989; Berrahma et al., 1993) if an exception is made for the one lava flow from Foum el Kouss that gave an age of 2.4 ± 0.1. The trachyandesite sample from Siroua yield an age of 2.8 ± 0.1 Ma. The three Saghro lavas from our study show progressively younger ages with increasing latitude, varying from 8.6 ± 0.3 Ma for the southernmost sample, for the Tlassem lava flows (AA13) to 5.4 ± 0.2 Ma, for the Ait Koukdene lavas (AA17), and 2.4 ± 0.1 Ma in the northernmost sector in the Ouarzazate basin, for the Foum el Kouss lava flows (AA21).

The studied volcanic rocks from Siroua and Saghro are alkaline, ranging from slightly (CIPW: *ne* = 2.21%–7.85%) to mildly (CIPW: *ne* = 13.9%–22.5%) silica-undersaturated, respectively. The samples from the Siroua volcanic field (Figure 5; diamonds) range in composition from trachyandesite to trachyte (Table S2). The trachyandesite (AA06) shows a porphyritic texture with phenocrysts represented by clinopyroxene, plagioclase, horneblende with opacitic rims, anorthoclase and rare olivine set in a microcrystalline intersertal groundmass mainly made of plagioclase and magnetite with subordinate clinopyroxene. Conversely, trachyte samples (i.e., AA03, AA04) are

15252027, 2023, 6, Downloaded from https://agupubs.onlinelibrary.wiley.com/doi/10.1029/2022GC010843 by Thorsten Becker - University Of Texas Libraries , Wiley Online Library on [12/06/2023]. See the Terms and Conditions (https://onlinelibrary.wiley.com/terms-and-conditions) on Wiley Online Library for rules of use; OA articles are governed by the applicable Creative Commons License

15252027, 2023, 6, Downloaded from https://agupubs.onlinelibrary.wiley.com/doi/10.1029/2022GC010843 by Thorsten Becker - University Of Texas Libraries , Wiley Online Library on [12/06/2023]. See the Terms and Conditions (https://onlinelibrary.wiley.com/terms-and-conditions) on Wiley Online Library for rules of use; OA articles are governed by the applicable Creative Commons License

characterized by porphyritic texture with large anorthoclase phenocrysts and subordinate clinopyroxene, biotite, and opaque microphenocrysts, set in a groundmass of alkali feldspar, magnetite, and clinopyroxene.

Samples from the Saghro volcanic field (Figure 5; triangles) range in composition from olivine nephelinites through clinopyroxene nephelinite (ankaramite of Foum el Kouss) to phonolites (Table S2). Olivine nephelinitic lavas (i.e., AA13, AA14, AA15, and AA17) have sub-porphyritic to porphyritic textures, with abundant euhedral to subhedral olivine (15–20 vol.%) with subordinate clinopyroxene phenocrysts (AA17) set in a microcrystalline groundmass made of nepheline, clinopyroxene, olivine, and opaques. Samples from Ait Koukdene (i.e., AA 17) and Tlassem (i.e., AA13-15) show the occurrence of small phleocroic tiny crystals recalling the optical feature of biotite in the groundmass. Clinopyroxene nephelinitic lavas are from the northernmost flows of Foum el Kouss (i.e., AA18, AA19, AA20, and AA21) and they are characterized by porphyritic textures with intense weathering features, with exception AA21 being one of the most fresh samples collected. In altered samples, olivine phenocrysts are often completely to partially transformed in iddingsite with clinopyroxene showing deep weathering and in the groundmass, showing abundant voids filled with secondary minerals (particularly in sample AA20). Samples AA19 show the highest PI with the occurrence of centimetric subhedral nepheline crystals with resorbed rims as well as by "holly leaf" spinel. The two phonolite samples from Saghro volcanic Field (i.e., Iknouen: AA22 and AA23) are characterized by strongly porphyritic texture with large alkali-feldspar phenocrysts followed by idiomorphic nepheline and sanidine microphenocrysts. Glomeroporhyritic aggregates of tabular alkali feldspar and acicular pale green clinopyroxene crystals are also present. The microcrystalline groundmass is composed of sanidine, nepheline, rare clinopyroxene, and opaque minerals. Sample AA22 shows a pilotaxitic texture of the groundmass with aligned sanidine microcrystals.

The most undifferentiated Saghro lavas show the typical features of near-primary melts (Mg# 65–73, Ni 140–290 ppm, Cr 230–490 ppm, Co 41–54 ppm, Sc 22–25 ppm; Frey et al., 1978) and the direct derivation of the phonolite lavas from nephelinite magma through differentiation by fractional crystallization was already demonstrated by (Berger, Ennih, et al., 2009).

Indications on the magmatic affinity, the mantle source composition and the melting conditions were retrieved by petrographic observation, major and trace element composition, Sr-Nd-Pb isotopic ratios, and REE distribution of the least differentiated igneous products (Figures 6–8). The new results indicate that the Anti Atlas alkaline mafic lavas of Saghro are characterized by the least radiogenic Sr ($^{87}Sr/^{86}Sr_i$ = 0.70300–0.70316) and unradiogenic Nd ($^{143}Nd/^{144}Nd_i$ = 0.51285–0.51289) of the entire Anti-Atlas volcanic sector. Saghro mafic lavas have initial Pb isotopic compositions in the ranges of 19.397–19.587, 15.596–15.654, and 38.994–39.341 for $^{206}Pb/^{204}Pb_i$, $^{207}Pb/^{204}Pb_i$, and $^{208}Pb/^{204}Pb_i$, respectively. Siroua youngest lavas have initial Pb isotopic compositions in the ranges of 19.173–19.401, 15.593–15.599, and 39.195–39.503 for $^{206}Pb/^{204}Pb_i$, $^{207}Pb/^{204}Pb_i$, and $^{208}Pb/^{204}Pb_i$, respectively. This implies the involvement of the HIMU (high $^{238}U/^{204}Pb$) component in the source of nephelinites with negligible influence of enriched mantle (EM) end-members (Figures 6 and 7b; Hofmann, 1997). The incompatible element distribution shows negative anomalies in K, Zr, Hf, and Ti for the Saghro mafic samples, typical of anorogenic magmas originating from a mantle source metasomatized by a carbonatitic component (Figure 7). Their REE distribution is characterized by high La/Yb (between 43 and 59.5) and Dy/Yb (between 2.9 and 3.3) ratios, compatible with a generation by very low degree of melting (0.5%–1.0%) of a LREE-enriched lherzolite (AZ7, Natali et al., 2013) mantle source containing 2% spinel and 1% garnet (Figure 8).

In summary, the petrographic, geochemical and isotopic characteristics of the studied Saghro and Siroua lavas imply that they were generated by various melting degrees of a lithospheric mantle source affected by carbonatite metasomatism. The occurrence of carbonatite nodules, together with several mineral phases (such as Ba-Ti biotite; Ibhi & Nachit, 2000) typical of alkaline-carbonatite complexes, in nephelinite from Saghro (Berger, Ennih, et al., 2009) represents petrographic evidence of their extremely high silica undersaturation which is in turn related to the very low melting degree.

4. Discussion

4.1. Origin of Miocene Magmatism

The Moroccan volcanism of the Miocene depicts an overall anorogenic signature, but it outcrops primarily along deformation belts. This feature renders the origin of magmatism a fundamental aspect to discern. Here, we combine our geochemical and isotopic data from the Anti Atlas volcanism into a broader context including the

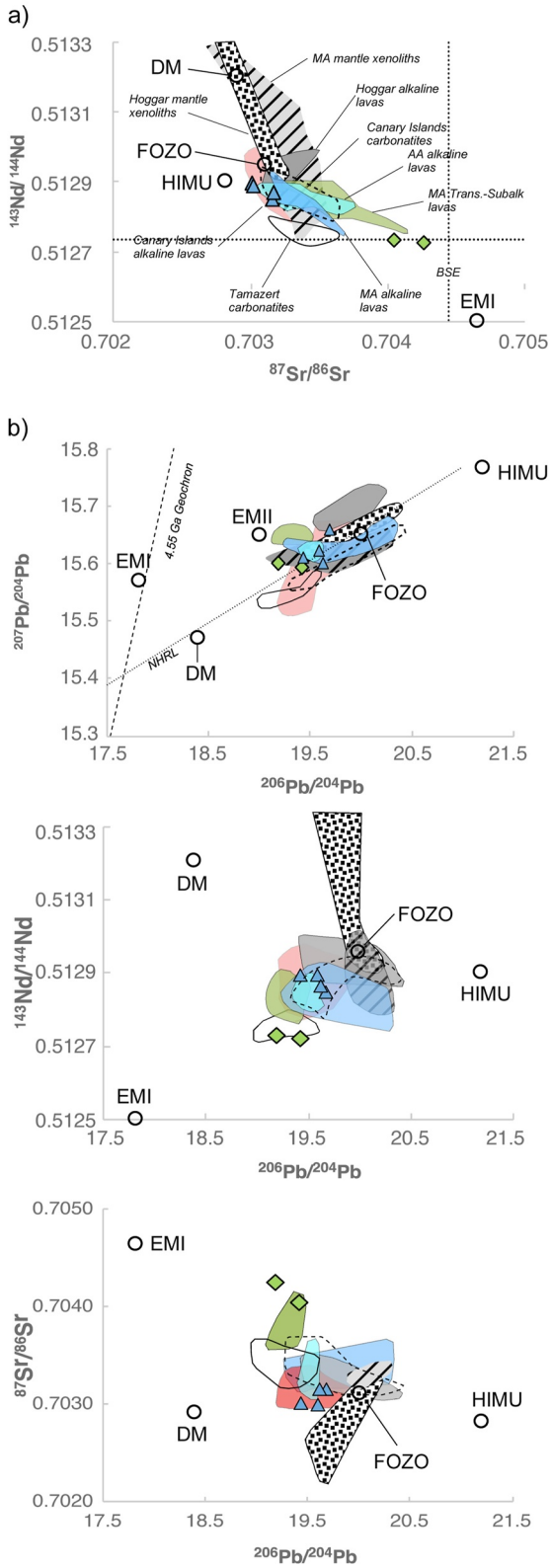

Figure 6.

15252027, 2023, 6, Downloaded from https://agupubs.onlinelibrary.wiley.com/doi/10.1029/2022GC010843 by Thorsten Becker - University Of Texas Libraries , Wiley Online Library on [12/06/2023]. See the Terms and Conditions (https://onlinelibrary.wiley.com/terms-and-conditions) on Wiley Online Library for rules of use; OA articles are governed by the applicable Creative Commons License

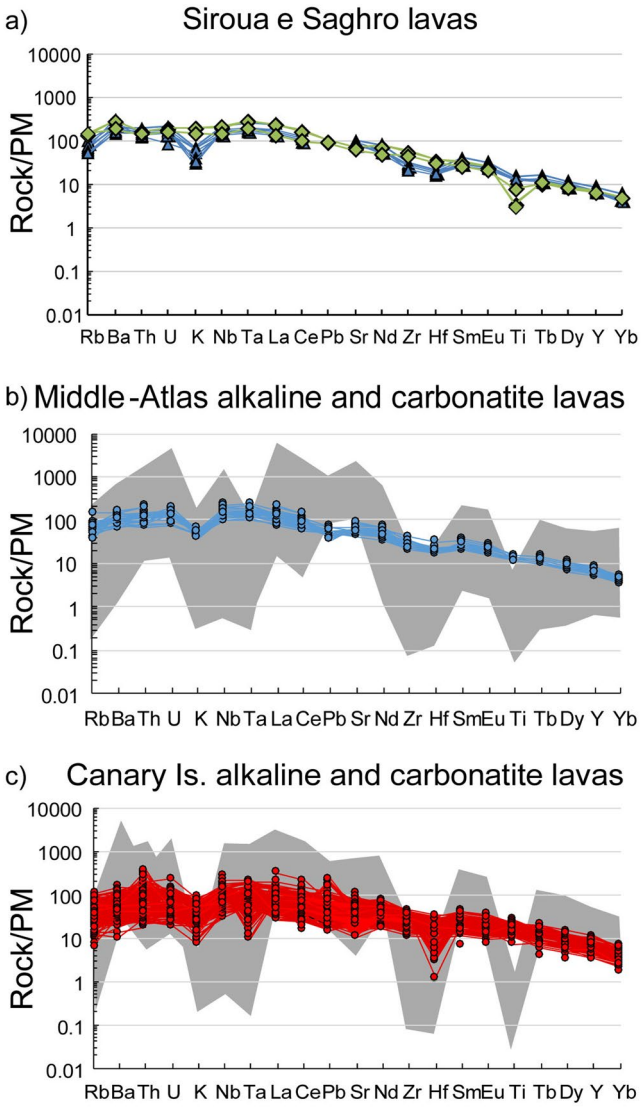

Figure 7. PM-normalized incompatible element distributions of the Saghro (blue) and Quaternary period of the Siroua (green) lavas from this study (a), in comparison with Middle Atlas (blue) and Canary Islands (red) mafic alkaline and carbonatite (gray) volcanics (b and c). Middle Atlas data from El Azzouzi et al. (2010) and Duggen et al. (2009). Canary Islands data from Ablay et al. (1998), Wolff et al. (2000), Carracedo et al. (2001), Lundstrom et al. (2003), Gurenko et al. (2006), Prægel and Holm (2006), Parat et al. (2011), Marti et al. (2013), Barker et al. (2015), Turner et al. (2015), Gómez-Ulla et al. (2018), Kurzweil et al. (2019). Normalization values are from Sun and McDonough (1989).

whole Moroccan and Canarias volcanism (including also previous samples from Anti-Atlas, e.g., Berger, Liégeois, et al., 2009; Berrahma et al., 1993; Chamboredon, 2015; Delaloye, 1989). This compilation highlights similarities and differences between the Miocene magmatic processes along the Atlas system.

The isotopic composition of the Anti-Atlas magmas, close to the FOZO (FOcal ZOne) mantle end-member, is typical of the North African Cenozoic alkaline volcanic provinces, including the Moroccan Middle Atlas (Bosch et al., 2014; Duggen et al., 2009), the Algerian Hoggar (Aït-Hamou et al., 2000; Allègre et al., 1981; Maza et al., 1998), the Northeastern African volcanism (Sudan and Egypt; Lucassen et al., 2008, the Canary, Lustrino & Wilson, 2007), and the Cape Verde islands (GEOROC database; "https://georoc.eu").

According to magma source modeling (Figure 8), the generation of subalkaline and transitional magmatism for the Middle Atlas (Duggen et al., 2009; El Azzouzi et al., 2014, 2010) would require higher melting degrees (2%–5%) of a mantle source similar to that inferred for Saghro and Middle Atlas alkaline lavas. The anorogenic Rif magmas are compatible with a genesis using similar source and melting conditions of the Sahgro and Middle Atlas alkaline lavas (Figure 7; Guilliz, Oujida, Gourougou; Duggen et al., 2005; El Azzouzi et al., 2010), with the exception of three samples showing very high Dy/Yb (3.6–3.8), which are compatible with generation from a deeper, spinel-free, mantle source (Figure 8). However, lavas from the Canary Island show the lowest Dy/Yb values, consistent with generation by 1%–10% melting degree of a garnet-free mantle source (Figure 7).

Geochemical modeling suggests that alkaline lavas from the Saghro and the Middle Atlas are generated at the garnet-spinel transition depth, which generally occurs around 2.5–2.7 GPa (80–85 km, Klemme & O'Neill, 2000; Robinson & Wood, 1998). Moreover, geochemical data indicate that the peridotite mantle source was characterized by the presence of accessory amphibole (model details in Supporting Information S1). Studies of experimental petrology have shown that basanites and nephelinites can be produced by melting a garnet or spinel peridotite containing amphibole and/or phlogopite at pressures above 2 GPa and at temperatures above 1,360°C in the presence of CO_2 (Dasgupta et al., 2007; Hirose, 1997; Mysen & Kushiro, 1977). However, it has also been shown that the production of basanites and nephelinites is also possible at lower temperatures of 1,200°C–1,250°C and at higher pressures of 2.8–3.0 GPa (Mengel & Green, 1986; Thibault et al., 1992). The presence of CO_2 during melting significantly reduces the SiO_2 content of the liquid produced by a peridotite due to crystallization of orthopyroxene coupled with the dissolution of olivine (e.g., Brey & Green, 1977; Falloon & Green, 1989; Gudfinnsson & Presnall, 2005; Kushiro, 1975; Wyllie & Huang, 1976). These experimental data, combined with the geochemical modeling results, suggest that the Saghro alkaline lavas result from the melting of a peridotite at the level of the garnet-spinel transition at pressures around 2.5–2.7 GPa and temperatures of 1,200°C–1,300°C. The presence of

Figure 6. (Sr-Nd-Pb isotopes)—(a) Sr-Nd and (b) Pb isotopic composition of anorogenic volcanism from the Saghro (Berger et al., 2014), Middle Atlas (Duggen et al., 2009; El Azzouzi et al., 2010) and Rif (Duggen et al., 2005; El Azzouzi et al., 1999, 2014) volcanic occurrences. The isotopic composition of Canary Islands volcanism derived from Georoc (http://georoc.mpch-mainz.gwdg.de/georoc/) is also reported for comparison. The gray-hatched field represents the composition of mantle xenoliths from the Middle Atlas (Natali et al., 2013; Raffone et al., 2009; Wittig, Pearson, Baker, et al., 2010; Wittig, Pearson, Duggen, et al., 2010). Isotopic mantle end members (DM, HIMU, EMI, and EMII) are reported after Zindler and Hart (1986). CHUR (Chondrite Uniform Reservoir) and UR (Uniform Reservoir) are reported as estimates of the bulk earth composition (Faure, 2013). Blue triangles indicate our samples from Sagrho while green diamonds represent our samples from Siroua.

15252027, 2023, 6, Downloaded from https://agupubs.onlinelibrary.wiley.com/doi/10.1029/2022GC010843 by Thorsten Becker - University Of Texas Libraries , Wiley Online Library on [12/06/2023]. See the Terms and Conditions (https://onlinelibrary.wiley.com/terms-and-conditions) on Wiley Online Library for rules of use; OA articles are governed by the applicable Creative Commons License

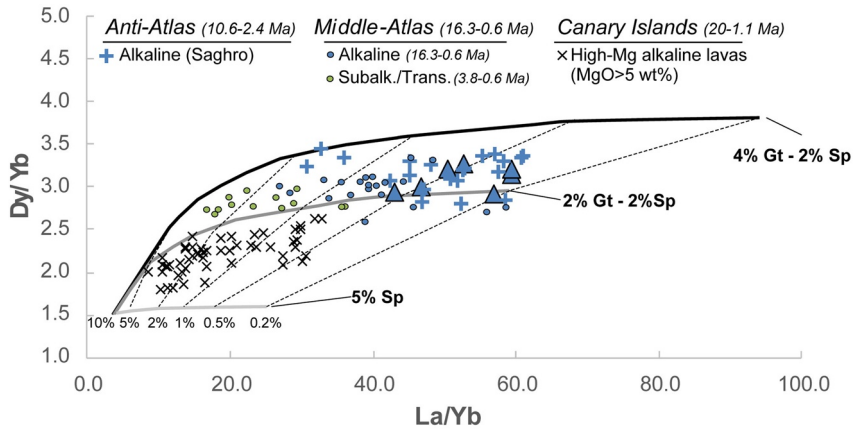

Figure 8. Magma source modeling. La/Yb versus Dy/Yb of the near primary anorogenic lavas from the Anti Atlas (Saghro and Siroua, data from this work and from Berger, Ennih, et al., 2009; Berger et al., 2014; Chamboredon, 2015), the Middle Atlas (Duggen et al., 2009; El Azzouzi et al., 2010) and the Rif (Duggen et al., 2005; El Azzouzi et al., 1999, 2014). Data from Canary Islands volcanism derived from Georoc are also reported for comparison. Non-modal fractional melting curves of the Azrou (Middle Atlas) LREE-enriched mantle xenolith AZ7 (Natali et al., 2013) with various Sp-Gt proportions are from Chamboredon (2015). Blue triangles indicate samples from this study.

amphibole in the residue and the low degrees of fusion (0.6%–2.5%) suggested by the model are in agreement with melting at relatively low temperatures (Jung & Hellebrand, 2006).

Our compilation suggests that the first Neogene magmatic cycle (16–9 Ma) along the Middle and Anti Atlas was characterized by the lowest melting degree of mantle sources located at various depths (deeper source for the Anti Atlas mantle source). A second magmatic cycle (8–0.7 Ma) was characterized by a progressive increase in the melting degree (more effective in the Middle Atlas). At this time, mantle sources are located at comparable depths, reaching the maximum in the last magmatic episodes of the Middle Atlas with the generation of transitional to subalkaline lavas.

4.2. Origin of Topography

The limited amount of shortening (see Arboleya et al., 2004; Domenech et al., 2018; Lanari et al., 2020a; Teixell et al., 2003), which primarily focuses on oblique-slip faults that do not produce crustal thickening alone suggests that the Atlas system high topography cannot be explained by pure local isostasy. Admittance analysis, free-air gravity variations, filtered topography at 150 km, and residual topography discussed here and in previous works (e.g., Craig et al., 2011; Miller & Becker, 2014) together support this conclusion. Interestingly, topographic anomalies also show a similar SW-NE pattern beneath the Miocene volcanic fields spread over Morocco (Figures 3 and 4). Thus, to first order, the long-wave length topography of the Atlas may indeed reflect a deeper mantle signal.

Figure 9 shows three swath profiles together with upper lithospheric sections and residual topography across the High, Anti, and Middle Atlas. Along the AA' section, 10–50 km filtered topographies are higher than those of section BB'. By contrast, the 100–150 km smoothed topographies show the inverse relation. In the CC' section, across the eastern High and Middle Atlas, the filtered and current topographies are generally lower compared to the AA' and BB' sections. These data suggest that the long wavelength-filtered topographies may capture deeper mantle contributions mainly over the Central High Atlas. On the contrary, the WHA shows a pronounced short wavelength crustal structure dominated by steep oblique–slip faults (Lanari et al., 2020a). Overall, the long wavelength topography (150 km) resembles the shape of the residual topography, with a maximum amplitude in correspondence to the Miocene Atlas volcanic fields (Figure 8). Positive residual topography suggests mantle processes for building the high topography, and the correspondence between high residual topography and magmatism moreover implies a linkage between dynamic topography and volcanism. In turn, volcanism must be linked with deformation as attested by (a) the observation that the Atlasic volcanism started during the middle Miocene together with a main deformation and cooling event (e.g., Lanari et al., 2020a, 2020b; Leprêtre et al., 2018); and (b) by Miocene Anti-Atlas volcanic deposit offset by oblique faults as documented by

15252027, 2023, 6, Downloaded from https://agupubs.onlinelibrary.wiley.com/doi/10.1029/2022GC010843 by Thorsten Becker - University Of Texas Libraries , Wiley Online Library on [12/06/2023]. See the Terms and Conditions (https://onlinelibrary.wiley.com/terms-and-conditions) on Wiley Online Library for rules of use; OA articles are governed by the applicable Creative Commons License

10.1029/2022GC010843

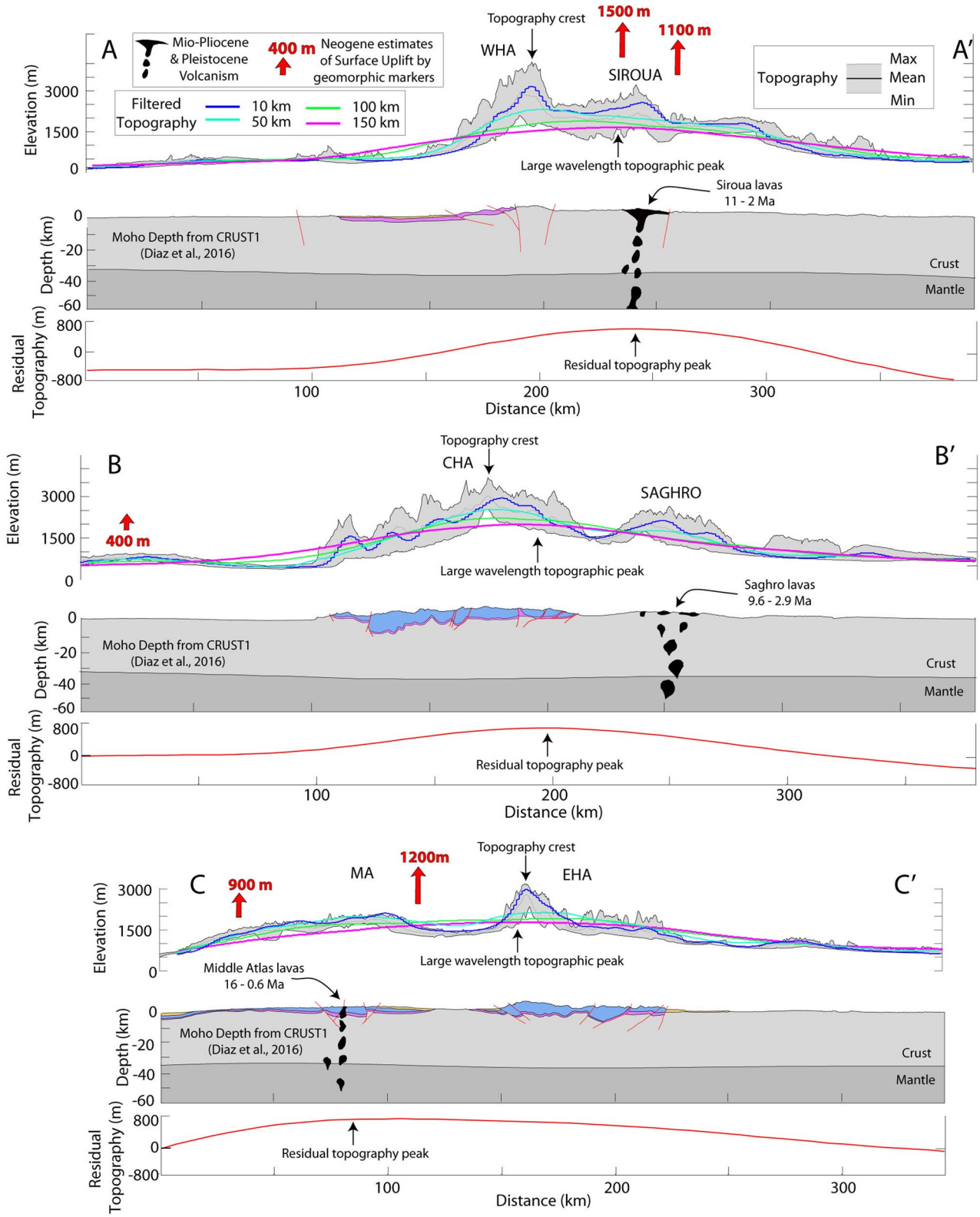

Figure 9. Topographic swath profiles (gray areas) with 50 km of window (see location in Figure 1) together with filtered topography profiles (see location in Figure 4), schematic lithospheric section with Moho depth according to CRUST1 and Díaz, Gil, et al. (2016) and residual topography (see section in Figure 4e). The residual topography is higher underneath the volcanic areas in (AA') (Western High Atlas) and (CC') (Eastern High Atlas) and between the volcanic area and the highest topography in (BB') (Central High Atlas). The Moho is everywhere at depths ≤30 km.

15252027, 2023, 6, Downloaded from https://agupubs.onlinelibrary.wiley.com/doi/10.1029/2022GC010843 by Thorsten Becker - University Of Texas Libraries , Wiley Online Library on [12/06/2023]. See the Terms and Conditions (https://onlinelibrary.wiley.com/terms-and-conditions) on Wiley Online Library for rules of use; OA articles are governed by the applicable Creative Commons License

15252027, 2023, 6, Downloaded from https://agupubs.onlinelibrary.wiley.com/doi/10.1029/2022GC010843 by Thorsten Becker - University Of Texas Libraries , Wiley Online Library on [12/06/2023]. See the Terms and Conditions (https://onlinelibrary.wiley.com/terms-and-conditions) on Wiley Online Library for rules of use; OA articles are governed by the applicable Creative Commons License

Lanari et al. (2020a). We conclude that the late Neogene Atlas evolution is affected by three main contributions coexisting during the same time: crustal deformation, volcanism, and mantle dynamics. Any model seeking to explain the origin of the current configuration of the Atlas orogeny should therefore consider the following constraints:

1. Crustal thickening is limited and cannot account for the topography elevation of the Atlas system.
2. Resumption of volcanism is contemporaneous with the acceleration of crustal deformation.
3. Long wavelength (>150 km) positive residual topography and free-air admittance variations suggest a dynamic deep mantle source.
4. Volcanism has anorogenic signatures involving a deep mantle source.

In the following section, we will discuss the previously proposed models, and by running simple physical tests, we propose a new model accounting for all the aforementioned considerations.

4.3. Previous Geodynamic Models

Based on various sets of observations, previous studies are accounted for the geodynamic origin of the anomalous topography of High Atlas. Namely, the surface topography and magmatism in the Atlas are considered to be driven by mantle upwelling(s) related to the Canary plume (Civiero et al., 2018; Duggen et al., 2009; Missenard et al., 2006), lithospheric thinning/removal (Ramdani, 1998), or a combination of both (Duggen et al., 2009; Missenard & Cadoux, 2012; Zeyen et al., 2005).

Delamination in the sense defined by Bird (1979), and Göğüş and Ueda (2018) where the mantle lithosphere slab peels back from beneath the crust has been proposed to explain the thin lithosphere beneath the Atlas and the overall geodynamic evolution of the western Mediterranean including the Alboran region (Anahnah et al., 2011; Baratin et al., 2016; Bezada et al., 2014; Palomeras et al., 2014). Note that the crustal-surface response of slab delamination may be different from viscous dripping (convective removal) as suggested for the evolution of the Alboran-western Mediterranean region (e.g., Platt & Vissers, 1989; Seber et al., 1996). Please see Göğüş and Psyklywec (2008) for the difference between the two. Such peeling back of the mantle lithosphere beneath the Atlas could explain the punctuated increase in buoyancy and uplift, and seems consistent with the geometry of the LAB. Receiver function analyses show that the LAB beneath the Central and Middle Atlas is at a depth of ∼75 km and is ∼30 km thinner than in the Sahara Craton and in the Meseta (Mancilla & Diaz, 2015; Miller & Becker, 2014; Miller et al., 2015). Low seismic velocity anomalies at 50 km depth also show the presence of hot asthenospheric material filling mantle cavities beneath the Central and the Middle Atlas (Bezada et al., 2014; Sun et al., 2014). Inversion of the topography and geoid assuming isostasy show, expectedly, similar features with a LAB at depths of ∼90–80 km beneath the Atlas compared to ∼150 km beneath the Sahara plateau and the Meseta (Fullea et al., 2010). Relative velocity anomalies and the thin LAB might indeed be associated with delamination. However, while this process would result in a cool material sinking down into the asthenosphere (cf. Bezada et al., 2014; Duggen et al., 2009), and replacement of the lithosphere with the background asthenosphere, alone it would not explain an actively buoyant anomaly associated with a higher thermal response than typical asthenospheric mantle, for example, as inferred from the analysis of Sun et al. (2014). In addition, geodynamic models show that delamination preceded by thickening should involve a first phase of subsidence owing to slab pull forces exerted on the crust. This migratory and transient tectonic response is followed by uplift (Göğüş & Psyklywec, 2008; Memiş et al., 2020) and is not consistent with the evolution of the region since there is no observed record of subsidence based on stratigraphic analyses.

A mantle upwelling may well explain the anomalous uplift of the Atlas and the volcanism in the High and the Middle Atlases. Two sources of upwelling have been proposed. The first relates to a small-scale, edge-driven convection due to lithospheric thickness contrast along the passive margin (Fullea et al., 2010; Missenard & Cadoux, 2012; Missenard et al., 2006; Ramdani, 1998). The second relates to a small-scale hot anomaly (Teixell et al., 2005; Zeyen et al., 2005) perhaps associated with the inflow of material from the Canary plume (Duggen et al., 2009; Hoernle et al., 1995; Miller et al., 2015; Oyarzun et al., 1997). The latter model is supported by the composition of volcanism in the Atlas resembling those of Canary (Duggen et al., 2009). This model is also supported by seismic data showing a deep, low-velocity anomaly at shallow upper mantle depths (Miller et al., 2015; Sun et al., 2014) and deeply rooted beneath the Canary Islands (Civiero et al., 2018, 2020) from the upper mantle transition zone. In particular, Duggen et al. (2009) proposed that

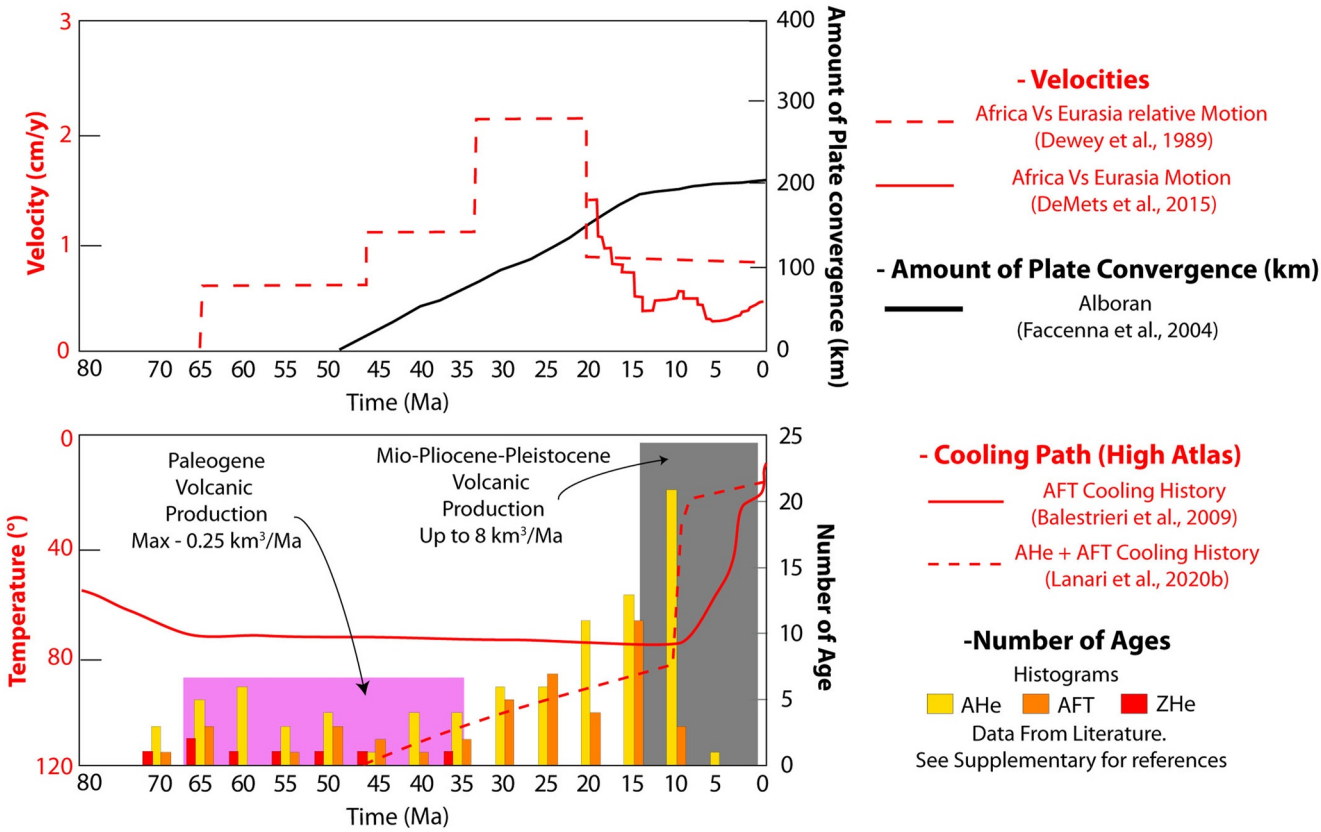

Figure 10. Comparison between the amount of plate convergence (Faccenna et al., 2004), velocity (DeMets et al., 2015; Dewey et al., 1989), cooling histories and histograms with numbers of cooling ages (listed in the compilation presented in Lanari, Boutoux, et al., 2023), together with the time emplacement of the two volcanic events in Morocco: Paleogene and Mio-Pliocene-Pleistocene. The plot of plate convergence and velocity is inspired by Missenard and Cadoux (2012).

a hot upwelling rising from the Canarias plume may be able to flow over large distances beneath the Atlas due to mantle suction produced by slab retreat and subsequent peeling/delamination in the Mediterranean (Mériaux et al., 2015).

Unfortunately, most of these studies focused on a single subset of data, leaving multiple open issues, which we seek to synthesize here comprehensively. For instance, why did the upwelling occur only since the Neogene and how can we explain the concurrence of crustal shortening, exhumation, and volcanism? As discussed above, the High Atlas deformed and exhumed primarily from the middle/late Miocene to the present, coevally with volcanism (e.g., Lanari et al., 2020a, 2020b; Missenard & Cadoux, 2012; Teixell et al., 2005). Although volcanism (and hence mantle upwelling) and the acceleration in exhumation occurred at the same time, the High Atlas exhumation is not a consequence of the long wavelength uplift. If this would be the case, younger cooling ages should dominate the Central High Atlas, where the major mantle contribution is focused (Figures 1 and 4), and not the WHA (Figures 1 and 4). Moreover, in the WHA, cooling ages get significantly older at short distances, especially crossing the axial oblique-slip faults highlighting a clear structural control (e.g., Lanari et al., 2020b).

Despite these considerations, the increase in exhumation since the middle/late Miocene is rather challenging to understand because it is a strict consequence of faulting acceleration (Lanari et al., 2020b). Such an acceleration is not supported by either an increase in the Africa/Eurasia plate convergence rate (DeMets et al., 2015; Dewey et al., 1989) nor by the total amount of convergence across the Alboran slab, which had been nearly stable over the last 15 Ma (Faccenna et al., 2004); Figure 10, inspired by Missenard and Cadoux (2012). It follows that the temporal linkage between volcanism and the increase in deformation and related exhumation may imply a causal connection (Figure 10).

15252027, 2023, 6, Downloaded from https://agupubs.onlinelibrary.wiley.com/doi/10.1029/2022GC010843 by Thorsten Becker - University Of Texas Libraries , Wiley Online Library on [12/06/2023]. See the Terms and Conditions (https://onlinelibrary.wiley.com/terms-and-conditions) on Wiley Online Library for rules of use; OA articles are governed by the applicable Creative Commons License

15252027, 2023, 6, Downloaded from https://agupubs.onlinelibrary.wiley.com/doi/10.1029/2022GC010843 by Thorsten Becker - University Of Texas Libraries , Wiley Online Library on [12/06/2023]. See the Terms and Conditions (https://onlinelibrary.wiley.com/terms-and-conditions) on Wiley Online Library for rules of use; OA articles are governed by the applicable Creative Commons License

4.4. Numerical Models

To explore the linkage between volcanism, surface uplift, and deformation, we analyzed a number of simple numerical models. These focus on potentially general processes and are not designed to investigate the regional setting in detail; models can thus only be broadly compared with the Atlas. Replicating the original shape of the Moho, or the exact geometry of the weak zones, for example, would be both challenging and possibly an overparameterization of the problem. However, our models provide first-order information on the way a mantle plume and volcanism might enhance deformation processes.

We test thermal plume and compression-related instabilities that are explored by time-dependent, 2-D, thermo-mechanical numerical models with parameters including for the compositional fields (i.e., thickness and density) provided in Table S1 and Figure S1a in Supporting Information S1. To solve the typical convection equations for the conservation of mass and momentum in the infinite Prandtl number regime, we use the ASPECT finite element code (ver. 2.2.0; Bangerth et al., 2020; Clevenger & Heister, 2021; Fraters et al., 2019; He et al., 2017; Heister et al., 2017; Kronbichler et al., 2012; Rose et al., 2017), considering visco-plastic rheology and incompressible fluids. Details of the numerical calculations including the rheological formulations are provided in the Appendix A. Any numerical model has to make simplifications, sometimes because of technical limitations, and more importantly and generally, to reduce complexity, and to be able to extract the basic underlying physics in hopefully general ways. Besides only considering 2-D cross sections, our simplifications include the neglecting of surface erosion and crustal heat production, which we consider of minor importance for the Atlas and expect to not lead to significant differences between the case studies. We also used a stabilization parameter for the quasi-free surface boundary, which leads to topographic smoothing (Kaus et al., 2010). Boundary conditions with the rates of the compression of the models (V_p) are shown in the supplementary material (Figures S1, S2, and S3 in Supporting Information S1). Plume–lithosphere interaction and the resultant variations at the boundaries (i.e., surface, Moho, and LAB) are the analyzed over the model evolution in terms of amplitudes, different shortening rates, and impingement times.

Figure 11 shows the numerical model results. Case "P" is a simple plume, cases "$S_{1–6}$" are shortening and the cases "$SP_{1–6}$" are a simple plume and shortening working at the same time. The indices identify the shortening rates: S_1 and SP_1 0.2 cm/yr, S_2 and SP_2 0.4 cm/yr, S_3 and SP_3 0.6 cm/yr, S_4 and SP_4 0.8 cm/yr, S_5 and SP_5 1 cm/yr and S_6 and SP_6 2 cm/yr. Each experiment lasts for 15 My, and we note the evolution of topography, crust, and lithosphere-asthenosphere boundary when the maximum elevation is reached (Figures 11a and 11b).

Our tests show that: (a) the upwelling mantle plume head modifies all anomaly patterns (uplift and crustal/lithospheric variations) since the isotropic compositional fields and depth-dependent homogenous background temperature have been used as the initial parameters in all plume-related, time-dependent models (Figures 11a and 11b). (b) Only plume-related evolution (P) creates higher topography (≥1 km) compared to the pure shortening model (S_i) where the topography, which is generally consistent with increasing shortening rates, never exceeds 0.7 km in S_6. The maximum topography is reached when a plume is combined with shortening, especially at high convergence rates (e.g., SP_4-SP_5-SP_6) (Figure 11c). This systematically occurs at 8 Ma since is the timing of the model mantle impingement. (c) In the models where a plume is combined with shortening (SP_i) the final topography and shapes, and the Moho and LAB discontinuities overall resemble the plume-only model (P) at long wavelengths. This indicates that the plume, with or without shortening, controls the subsurface deformations in P and SP_i by eroding the lower lithosphere with important consequences for the final topography shape and amplitude (Figures 11a and 11b). (d) In the experiments where the plume is active, with or without shortening (P or SP_i), the highest topography is achieved in half of the time with respect to the pure shortening-related experiments (S_i) (Figure 11d).

4.5. Potential Feedback Between Mantle Upwelling and Crustal Deformation: From Model to Nature

Our model focuses on the effects of compression and plume-related dynamic uplift and subsurface deformation and their possible effects on building topography. We infer that a mantle plume exerts a crucial control in shaping the topography and the deeper discontinuities (see conceptual model in Figure 12). Our plume model activates mechanisms similar to those that have long been investigated (e.g., Burov et al., 2007; Göğüş, 2020; Gurnis et al., 2000). As would be expected for a Stokes sphere, a number of models for plume dynamics suggest that the thermal plume radius and excess temperature have a significant impact on the resultant topography and melt

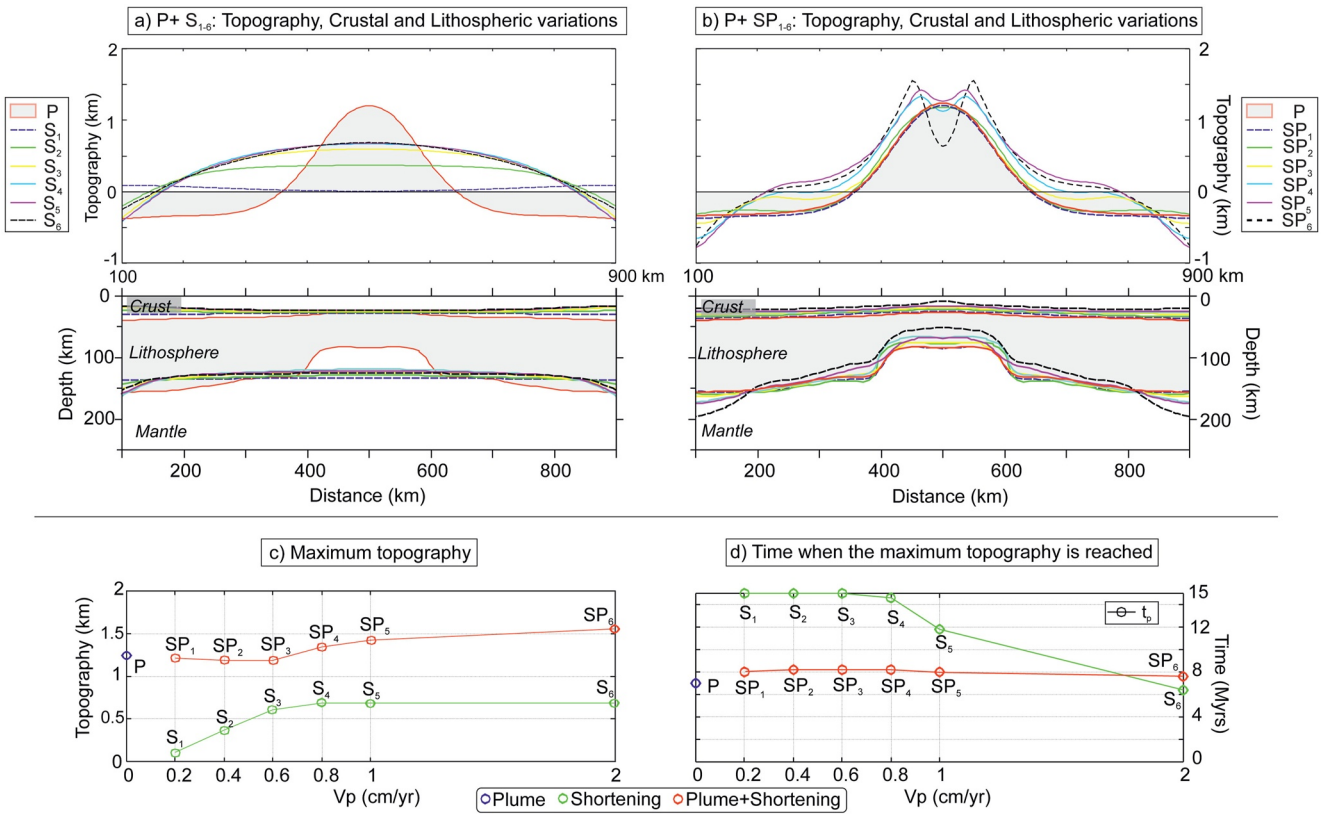

Figure 11. Estimations of dynamic uplift, crustal and lithospheric thicknesses obtained from different numerical modeling configurations: (a) P (plume-only) and S_i (shortening-only) (b) P and SP_i (plume + shortening models). (c) Variations of maximum surface uplift; (d) impingement time versus convergence rates based on the models listed in the text and Figure S1 in Supporting Information S1.

production rate (e.g., Wang et al., 2022). Similar to what was explored, for example, by Burov et al. (2007), we find that the plume arrival can trigger mantle lithospheric erosion, resulting in sharp discontinuities and lithospheric thinning. This lithospheric weakening might enhance the ongoing crustal deformation even for slow/constant convergence rates (see conceptual model in Figure 12).

We re-emphasize that our models are not designed to reproduce the Atlas in detail, but several features and general effects might resemble the natural case. Results, selected from a range of experiments, are qualitatively compared in terms of topographic, crustal, and LAB boundary evolution after mantle plume impingement and compression-related instabilities. The lithospheric thinning developed in our tests is quite sharp (Figure 11a), comparable with lithospheric features underneath the High Atlas as inferred from receiver functions (Miller & Becker, 2014). While many specifics are, of course, a direct function of our setup and initial condition, the models' topography wavelength is larger than 200 km, in agreement with our topographic analyses, and the depth of the lithosphere-asthenosphere boundary is ~85 km for both models and the natural case (Miller & Becker, 2014). This value is also similar to the depth estimated by geochemical modeling for the Saghro and Middle Atlas lavas to generate the garnet-spinel transition.

We use our model's predictions to speculate about the ongoing processes along the Atlas. We suggest that the progressive lithospheric thinning and weakening might serve to enhance crustal deformation over time. This would explain the inconsistency between local fault acceleration (e.g., Lanari et al., 2020b) and decreasing in the Africa/Eurasia convergence since the late Miocene (see also Missenard & Cadoux, 2012). Clearly, such a process can be affected by preexisting strength contrasts. Examples are *decollèment* layers in the WHA (Missenard et al., 2007) which localize the deformation mainly along the two-axial oblique-slip faults compared to the Central High Atlas where the deformation is instead accommodated over a broad region (Lanari et al., 2020b). Lastly, the coexisting contribution of lithospheric thinning, mantle upwelling, and reactivation of weakness zones might positively influence the crustal deformation which in turn serves to speed up exhumation.

15252027, 2023, 6, Downloaded from https://agupubs.onlinelibrary.wiley.com/doi/10.1029/2022GC010843 by Thorsten Becker - University Of Texas Libraries , Wiley Online Library on [12/06/2023]. See the Terms and Conditions (https://onlinelibrary.wiley.com/terms-and-conditions) on Wiley Online Library for rules of use; OA articles are governed by the applicable Creative Commons License

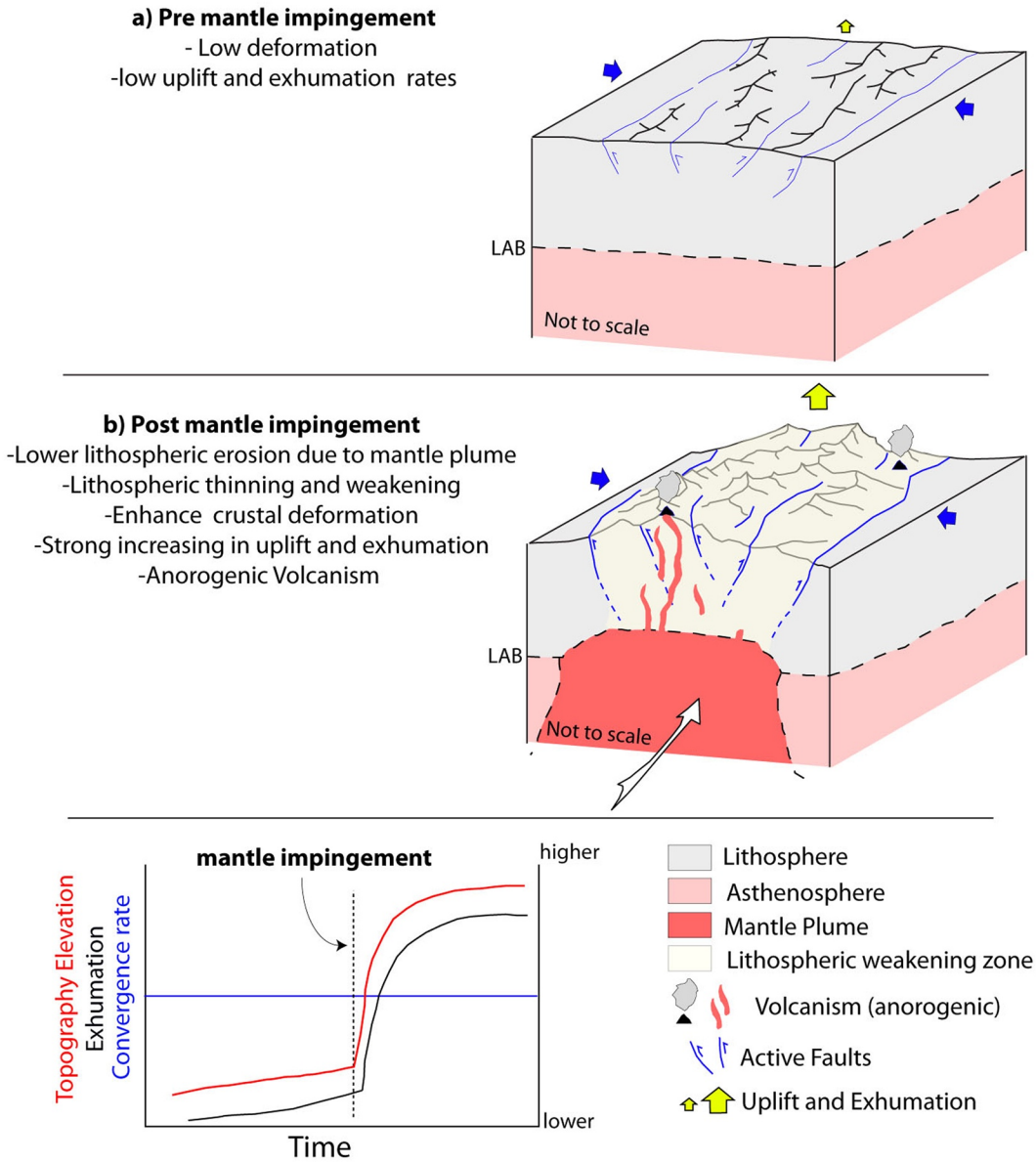

Figure 12. Schematic evolution model of the High and Anti Atlas for four different time intervals: (a) Oligocene-Miocene; Pre mantle impingement and (b) Miocene-Present; Post mantle impingement.

4.6. Pattern of Mantle Dynamics Below the Atlas-Betic System

The elongated shape of the long wavelength and residual topography (Figure 4) together with the results of the admittance analysis (Figure 3) and mantle anisotropy (Miller & Becker, 2014) support the hypothesis of asthenospheric material flowing underneath the Atlas (Duggen et al., 2009). We reconstruct the tectonic setting through time based on previous data and on our new constraints (Figure 13). We consider that: (a) crustal deformation and exhumation start during the middle/late Miocene, contemporaneous with the resumption of volcanism; (b) anorogenic volcanism has a deep source; (c) a dynamic and deep mantle source is required to support the high topography; and (d) mantle upwelling and crustal deformation operate simultaneously.

Our reconstruction starts at ~23 Ma (Figure 13a). At that time, the Gibraltar slab was retreating, producing an extension in the Alboran Sea, while most of the compressional deformation was concentrated along the Rif-Tell and Betics, with only small scale compressional pulses reported along the Atlas (Frizon de Lamotte et al., 2000, 2009; Leprêtre et al., 2018). Around 15 Ma (Figure 13b), the Gibraltar slab separated from the Algerian slab, which

15252027, 2023, 6, Downloaded from https://agupubs.onlinelibrary.wiley.com/doi/10.1029/2022GC010843 by Thorsten Becker - University Of Texas Libraries , Wiley Online Library on [12/06/2023]. See the Terms and Conditions (https://onlinelibrary.wiley.com/terms-and-conditions) on Wiley Online Library for rules of use; OA articles are governed by the applicable Creative Commons License

10.1029/2022GC010843

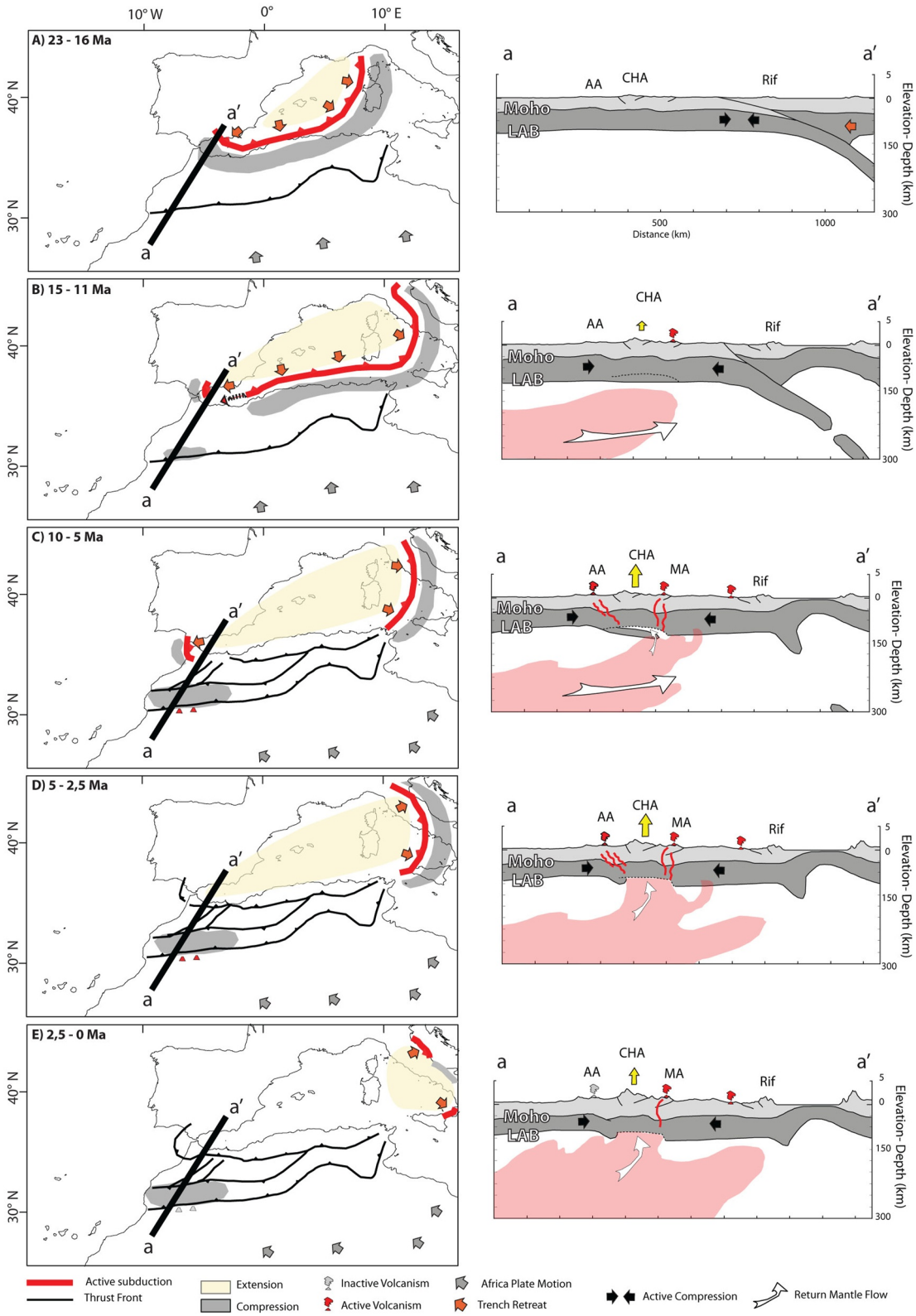

Figure 13. Schematic reconstruction of the evolution of the Western Mediterranean region since the Miocene inspired by Faccenna et al. (2004). The left column shows a schematic map and the right column shows the related schematic lithospheric sections. AA is the Anti Atlas, CHA is the Central High Atlas, and MA is the Middle Atlas.

15252027, 2023, 6, Downloaded from https://agupubs.onlinelibrary.wiley.com/doi/10.1029/2022GC010843 by Thorsten Becker - University Of Texas Libraries , Wiley Online Library on [12/06/2023]. See the Terms and Conditions (https://onlinelibrary.wiley.com/terms-and-conditions) on Wiley Online Library for rules of use; OA articles are governed by the applicable Creative Commons License

15252027, 2023, 6, Downloaded from https://agupubs.onlinelibrary.wiley.com/doi/10.1029/2022GC010843 by Thorsten Becker - University Of Texas Libraries , Wiley Online Library on [12/06/2023]. See the Terms and Conditions (https://onlinelibrary.wiley.com/terms-and-conditions) on Wiley Online Library for rules of use; OA articles are governed by the applicable Creative Commons License

turned inactive due to the entrance of thick continental African lithosphere at the trench (Faccenna et al., 2004). This likely produces a vertical tear, progressively opening a slab window. The Gibraltar slab was then free to retreat backward to the west because it became unlinked from the rest of the African slab (Faccenna et al., 2004).

This slab retreat would have produced toroidal flow that entered through the slab window (Diaz, Gallart, & Carbonell, 2016; Funiciello et al., 2006; Miller et al., 2015). As proposed, this mantle suction involved a broad region influencing the Canary mantle plume that since the late Miocene has started to flow northeastward (Duggen et al., 2009; Mériaux et al., 2015). This hot material, in turn, induced widespread volcanic activity from the late Miocene as documented in previous work and our compilation (see references in Supporting Information S1). The mantle upwelling eroded the lower lithosphere producing in turn thinning and weakening. As a result of the northward African plate convergence, compressional deformation localized along the weak part of the lithosphere, producing a surge of deformation and exhumation (Lanari et al., 2020a). The localization of convergence and inversion of the Atlas system at that time is consistent with the chocking and cessation of the Rif and Tell, inducing a southward jump to the weaker zone (Figure 13; Frizon de Lamotte et al., 2009).

The resulting topographic signal would have been expressed by the superimposition of a short wavelength crustal signal over a larger wavelength mantle dynamic signal. Whether this dynamic support underneath the Atlas continues to operate, inducing uplift, or if it vanished over the last few millions of years remains unclear (Lanari et al., 2022). In the Anti Atlas, for instance, no volcanic ages younger than 2 Myrs have been reported, while along the Middle Atlas, volcanism is active up to 0.6 Ma. Moreover, since the Quaternary, the Anti Atlas is characterized by high elevation valleys infilling processes possibly because of waning uplift rates (Lanari et al., 2022). Such an inference applies only to the Anti Atlas since the High Atlas is still clearly affected by active compression, as shown by seismotectonic analysis (Meghraoui et al., 1999; Sébrier et al., 2006). Compression and uplift in the High Atlas are also active throughout the Quaternary period as documented by faulted fluvial terraces and tilted Pleistocene deposits (Boulton et al., 2014; Pastor et al., 2012; Stokes et al., 2017).

Overall, our model thus substantiates the suggestion by Duggen et al. (2009) of a link between the Canary plume and the Atlas with the presence of horizontal mantle flow toward Gibraltar. Yet, some issues are left to be fully explored. In particular, the connections between the Gibraltar subduction zone, plume dynamics, and lithospheric thickness modifications remain to be explored with a comprehensive 3-D model. The asthenospheric setting with plume-slab interactions is perhaps similar to Samoa or Yellowstone (e.g., Kincaid et al., 2013) or the Afar-Hellenic system where slab segmentation has been suggested to assist in the northward flow of plume material underneath Arabia (e.g., Faccenna et al., 2013). Based on related analog modeling work, Mériaux et al. (2015) concluded that more than 1,500 km of mantle transport in the sub-lithospheric Atlas, captured by slab-roll back, is dynamically plausible.

However, our model differs from Duggen et al.'s (2009) model in important ways considering the role and timing of delamination. Duggen et al. (2009) suggested delamination to be the origin of a "*subcontinental lithospheric corridor*" and the cause for most of the shortening since ca. 45 Ma. Their long-lasting model also aimed to explain the Eocene anorogenic volcanism, which is well documented in Morocco. Such a volcanic episode is also anorogenic as the late Miocene one, but is not accompanied by an increase in shortening and exhumation. In light of the low temperature thermochronology cooling ages (cf. the compilation in Lanari et al., 2020b; Lanari, Boutoux, et al., 2023, and references therein) and morphological data (e.g., Babault et al., 2008; Clementucci et al., 2022, 2023a, 2023b), the Eocene and the late Miocene volcanisms require a different explanation. As discussed in Section 4.2, we show a strong increase in exhumation (which is deformation-related, as we previously discussed) and uplift since the middle/late Miocene, implying that this time represents the likely timing that we have to consider as an initial constraint for any geodynamic model. In addition, according to our numerical tests, the lithospheric thinning seen beneath the Atlas (e.g., Miller & Becker, 2014) can be caused by the erosion induced by active mantle upwelling, suggesting that delamination is not necessary to thin the lithosphere but may instead be the consequence of plume erosion.

Our model thus modifies Duggen et al.'s (2009) model, at least for the case of the Atlas, by emphasizing the possible feedback between plume-induced lithospheric weakening and strain localization (Figure 12). This process may be relevant for other convergent settings where deep mantle dynamics leads to volcanism during nappe stacking. Possible examples include the Caucasus or the Alborz belts where high topography formed during concurrently acting contributions of mantle convection effects, crustal deformation, and volcanism (see conceptual model in Figure 12).

15252027, 2023, 6, Downloaded from https://agupubs.onlinelibrary.wiley.com/doi/10.1029/2022GC010843 by Thorsten Becker - University Of Texas Libraries , Wiley Online Library on [12/06/2023]. See the Terms and Conditions (https://onlinelibrary.wiley.com/terms-and-conditions) on Wiley Online Library for rules of use; OA articles are governed by the applicable Creative Commons License

5. Conclusions

We explored the connection between crustal shortening, volcanism, and mantle dynamics along the Atlas. We provide a revision of tectonic and crustal evolution together with volcanism, combining the timing of deformation and the topographic evolution with new ages and petrographic properties from the Siroua and Saghro volcanic fields in the Anti Atlas. We combine this revision with a model to explore the interactions between mantle plume, volcanism, and crustal deformation processes in the Atlas system. Our results confirm a deep mantle source for explaining the late Neogene evolution of high topography, deformation, and volcanism. Moreover, late Neogene volcanism occurred contemporaneously with the main deformational events. Lastly, we explore the linkage between volcanism, surface uplift, and deformation by running numerical models to provide first-order information on the way mantle plumes and volcanism might enhance deformation processes. We conclude that if a mantle plume can erode the lower lithosphere, the resulting sharp/localized discontinuities might in turn weaken the lithosphere itself, and this may result in enhanced crustal deformation. This "*Plume-Assisted Orogeny*" process is expected to be enhanced along pre-exiting structural fabrics, explaining why, for instance, in the WHA the exhumation rates are faster even if the mantle contribution is lower with respect to the CHA.

Appendix A

The finite element code solves the system of convection equations describing the motion of a viscous fluid under the influence of the gravitational forces (Boussinesq approximation) without the effects of inertia (e.g., Bangerth et al., 2020, and references therein). The governing equations are for the conservation of mass, momentum, and energy, respectively:

$$\nabla \cdot v = 0 \tag{A1}$$

$$\nabla \cdot \sigma_{ij} + \rho g = 0 \tag{A2}$$

$$\rho C_p(\partial T/\partial t + v \cdot \nabla T) = k\nabla^2 T \tag{A3}$$

where v is velocity (m/s), g is gravitational acceleration (9.8 m/s^2), k is thermal conductivity (W/m/K), $\nabla T = T - T_0$ is temperature variation (K) (T_0: reference temperature), C_p is the specific heat capacity (J/kg/K), t is time (s) and σ is the stress tensor. Density: $\rho = \rho_0(1 - \alpha\nabla T)$, where ρ_0 is reference density (Table A1) and α is thermal expansivity (2×10^{-5} 1/K). We include plastic yielding using a Drucker-Prager criterion (similar to Mohr Coulomb) for the deformation associated with the quasi-frictional plastic yield stress (e.g., Glerum et al., 2018 and references therein, Table A1). Accordingly, we consider the deviatoric stress; $\sigma'_{ij} = \min\{\sigma_y; \sigma_v\}$ based on the plastic yield stress ($\sigma_y = p\sin\varphi$, φ is the internal angle of friction, p is total pressure, Pa) and the viscous stress ($\sigma_v = 2\eta_e\dot{\varepsilon}$). The viscous deformation is governed by non-Newtonian power law creep based on the temperature and the strain rate tensor ($\dot{\varepsilon}$); $\eta_e(\dot{\varepsilon}, T) = A^{-1/n}\dot{\varepsilon}^{(1/n-1)}e^{(Q+pV)/nRT}$, where η_e is effective viscosity, R is the gas constant (8.31 J/mol/K), n the power law exponent, Q is activation energy, V is activation volume, and A is the viscosity parameter (Table A1, e.g., Gleason & Tullis, 1995; Hirth & Kohlstedt, 1996; Naliboff & Buiter, 2015; Ranalli, 1995).

Table A1
Reference Parameters for the Numerical Modeling (e.g., Faccenna & Becker, 2020; Gleason & Tullis, 1995; Hirth & Kohlstedt, 1996; Naliboff & Buiter, 2015; Ranalli, 1995)

	Crust (wet qtz.)	Mantle lithosphere (dry olivine)	Asthenospheric mantle (dry olivine)
Density (kg/m^3)	2,775	3,250	3,210
Viscosity pre-factor (A; Pa^{-n}/s)	1.1×10^{-28}	4.85×10^{-17}	4.85×10^{-17}
Power exponent (n)	4	3.5	3.5
Activation energy (Q; kJ/mol)	223	530	530
Thermal conductivity (k; W/m/K)	2.5	2.25	2.25

Note. The internal friction angle ($\varphi = 20°$) and the specific heat capacity (C_p = 750 J/kg/K) are same for all materials. Activation volumes (V) = 18×10^{-6} (m^3/mol) for the materials beneath the crust. The reference strain rate = 1×10^{-14} 1/s, the viscosity limits are $\eta_e = 1 \times 10^{19}$–$5 \times 10^{21}$ Pas.

Data Availability Statement

The free-air gravity and topography data are constructed using Earth Gravitational Model 2012 (Bonvalot et al., 2012; https://bgi.obs-mip.fr/data-products/grids-and-models/wgm2012-global-model/). Supplementary information including detail descriptions of the methods, also including tables with location and results of the petrographic data are available at "https://osf.io/mwcbq" Lanari (2023).

Acknowledgments
The authors warmly thank Paolo Ballato, Frank Pazzaglia and Maria Laura Balestrieri for the inspiring discussions concerning the evolution of the Atlas system over the years. We acknowledge the reviewer Ioannis Baziotis and an anonymous reviewer for their comments and criticism that significantly improved the manuscript and the Editor Paul Asimow for constructive suggestions. TWB was partially supported by NSF EAR Grants 2045292 and 1925939. We thank the Computational Infrastructure for Geodynamics (https://geodynamics.org/), which is funded by the National Science Foundation under award EAR-0949446 and EAR-1550901 for supporting the development of ASPECT.

References

Ablay, G. J., Carroll, M. R., Palmer, M. R., Martí, J., & Sparks, R. S. J. (1998). Basanite–phonolite lineages of the Teide–Pico Viejo volcanic complex, Tenerife, Canary Islands. *Journal of Petrology*, *39*(5), 905–936. https://doi.org/10.1093/petroj/39.5.905

Aït-Hamou, F., Dautria, J.-M., Cantagrel, J.-M., Dostal, J., & Briqueu, L. (2000). Nouvelles données géochronologiques et isotopiques sur le volcanisme cénozoïque de l'Ahaggar (Sahara algérien): Des arguments en faveur de l'existenced'un panache. *Comptes Rendus de l'Academie des Sciences Series IIA: Earth and Planetary Science*, *330*(12), 829–836. https://doi.org/10.1016/s1251-8050(00)00217-2

Allègre, C. J., Dupré, B., Lambret, B., & Richard, P. (1981). The subcontinental versus suboceanic debate, I Lead-neodymium-strontium isotopes in primary alkali basalts from a shield area the Ahaggar volcanic suite. *Earth and Planetary Science Letters*, *52*(1), 85–92. https://doi.org/10.1016/0012-821x(81)90210-7

Anahnah, F., Galindo-Zaldívar, J., Chalouan, A., Pedrera, A., Ruano, P., Pous, J., et al. (2011). Deep resistivity cross section of the intraplate Atlas Mountains (NW Africa): New evidence of anomalous mantle and related Quaternary volcanism. *Tectonics*, *30*(5), 1–9. https://doi.org/10.1029/2010TC002859

Arboleya, M.-L., Babault, J., Owen, L. a., Teixell, a., & Finkel, R. C. (2008). Timing and nature of Quaternary fluvial incision in the Ouarzazate foreland basin, Morocco. *Journal of the Geological Society*, *165*(6), 1059–1073. https://doi.org/10.1144/0016-76492007-151

Arboleya, M. L., Teixell, A., Charroud, M., & Julivert, M. (2004). A structural transect through the high and middle Atlas of Morocco. *Journal of African Earth Sciences*, *39*(3–5), 319–327. https://doi.org/10.1016/j.jafrearsci.2004.07.036

Ayarza, P., Alvarez-Lobato, F., Teixell, A., Arboleya, M. L., Tesón, E., Julivert, M., & Charroud, M. (2005). Crustal structure under the central High Atlas Mountains (Morocco) from geological and gravity data. *Tectonophysics*, *400*(1–4), 67–84. https://doi.org/10.1016/j.tecto.2005.02.009

Ayarza, P., Carbonell, R., Teixell, A., Palomeras, I., Martí, D., Kchikach, A., et al. (2014). Crustal thickness and velocity structure across the Moroccan Atlas from long offset wide-angle reflection seismic data: The SIMA experiment. *Geochemistry, Geophysics, Geosystems*, *15*(5), 1698–1717. https://doi.org/10.1002/2013gc005164

Azdimousa, A., Bourgois, J., Poupeau, G., Vazquez, M., Asebriy, L., & Labrin, E. (2014). Fission track thermochronology of the Beni Bousera peridotite massif (Internal Rif, Morocco) and the exhumation of ultramafic rocks in the Gibraltar Arc. *Arabian Journal of Geosciences*, *7*(5), 1993–2005. https://doi.org/10.1007/s12517-013-0924-3

Babault, J., Teixell, A., Arboleya, M. L., & Charroud, M. (2008). A late Cenozoic age for long-wavelength surface uplift of the Atlas Mountains of Morocco. *Terra Nova*, *20*(2), 102–107. https://doi.org/10.1111/j.1365-3121.2008.00794.x

Balestrieri, M. L., Moratti, G., Bigazzi, G., & Algouti, A. (2009). Neogene exhumation of the Marrakech High Atlas (Morocco) recorded by apatite fission-track analysis. *Terra Nova*, *21*(2), 75–82. https://doi.org/10.1111/j.1365-3121.2008.00857.x

Ballato, P., Uba, C. E., Landgraf, A., Strecker, M. R., Sudo, M., Stockli, D. F., et al. (2011). Arabia-Eurasia continental collision: Insights from late Tertiary foreland-basin evolution in the Alborz Mountains, northern Iran. *Bulletin*, *123*(1–2), 106–131. https://doi.org/10.1130/b30091.1

Bangerth, W., Dannberg, J., Gassmoeller, R., & Heister, T. (2020). ASPECT v2. 2.0. *Zenodo*. Retrieved from https://zenodo.org/record/3924604

Baratin, L. M., Mazzotti, S., Chéry, J., Vernant, P., Tahayt, A., & Mourabit, T. (2016). Incipient mantle delamination, active tectonics and crustal thickening in Northern Morocco: Insights from gravity data and numerical modeling. *Earth and Planetary Science Letters*, *454*, 113–120. https://doi.org/10.1016/j.epsl.2016.08.041

Barbero, L., Jabaloy, A., Gómez-Ortiz, D., Pérez-Peña, J. V., Rodríguez-Peces, M. J., Tejero, R., et al. (2011). Evidence for surface uplift of the Atlas Mountains and the surrounding peripheral plateaux: Combining apatite fission-track results and geomorphic indicators in the Western Moroccan Meseta (coastal Variscan Paleozoic basement). *Tectonophysics*, *502*(1–2), 90–104. https://doi.org/10.1016/j.tecto.2010.01.005

Barbero, L., Teixell, A., Arboleya, M. L., del Río, P., Reiners, P. W., & Bougadir, B. (2007). Jurassic-to-present thermal history of the central High Atlas (Morocco) assessed by low-temperature thermochronology. *Terra Nova*, *19*(1), 58–64. https://doi.org/10.1111/j.1365-3121.2006.00715.x

Barker, A. K., Troll, V. R., Carracedo, J. C., & Nicholls, P. A. (2015). The magma plumbing system for the 1971 Teneguía eruption on La Palma, Canary Islands. *Contributions to Mineralogy and Petrology*, *170*(5–6), 1–21. https://doi.org/10.1007/s00410-015-1207-7

Baziotis, I., Xydous, S., Asimow, P. D., Mavrogonatos, C., Flemetakis, S., Klemme, S., & Berndt, J. (2019). The potential of phosphorus in clinopyroxene as a geospeedometer: Examples from mantle xenoliths. *Geochimica et Cosmochimica Acta*, *266*, 307–331. https://doi.org/10.1016/j.gca.2019.04.024

Beauchamp, W., Allmendinger, R. W., Barazangi, M., Demnati, A., El Alji, M., & Dahmani, M. (1999). Inversion tectonics and the evolution of the High Atlas Mountains, Morocco, based on a geological-geophysical transect. *Tectonics*, *18*(2), 163–184. https://doi.org/10.1029/1998TC900015

Berger, J., Ennih, N., & Liégeois, J.-P. (2014). Extreme trace elements fractionation in Cenozoic nephelinites and phonolites from the Moroccan Anti-Atlas (Eastern Saghro). *Lithos*, *210*, 69–88. https://doi.org/10.1016/j.lithos.2014.09.018

Berger, J., Ennih, N., Liégeois, J.-P., Nkono, C., Mercier, J.-C. C., & Demaiffe, D. (2008). A complex multi-chamber magmatic system beneath a late Cenozoic volcanic field: Evidence from CSDs and thermobarometry of clinopyroxene from a single nephelinite flow (Djbel Saghro, Morocco). *Geological Society, London, Special Publications*, *297*(1), 509–524. https://doi.org/10.1144/sp297.25

Berger, J., Ennih, N., Mercier, J.-C., Liégeois, J.-P., & Demaiffe, D. (2009). The role of fractional crystallization and late-stage peralkaline melt segregation in the mineralogical evolution of Cenozoic nephelinites/phonolites from Saghro (SE Morocco). *Mineralogical Magazine*, *73*(1), 59–82. https://doi.org/10.1180/minmag.2009.073.1.59

Berger, J., Liégeois, J., Ennih, N., & Bonin, B. (2009). Flow of Canary mantle plume material through a subcontinental lithospheric corridor beneath Africa to the mediterranean: Comment 30516. https://doi.org/10.1130/G30516C.1

Berrahma, M., & Delaloye, M. (1989). Données géochronologiques nouvelles sur le massif volcanique du Siroua (Anti-Atlas, Maroc). *Journal of African Earth Sciences*, *9*(3–4), 651–656. https://doi.org/10.1016/0899-5362(89)90049-3

Berrahma, M., Delaloye, M., Faure-Muret, A., & Rachdi, H. E. N. (1993). Premières données géochronologiques sur le volcanisme alcalin du Jbel Saghro, Anti-Atlas, Maroc. *Journal of African Earth Sciences*, *17*(3), 333–341. https://doi.org/10.1016/0899-5362(93)90077-4

Berrahma, M., & Hernandez, J. (1985). Nouvelles donnees sur le volcanisme trachytique hyperalcalin du volcan du Siroua (Anti-Atlas, Maroc). Comptes rendus de l'Académie des sciences. *Série 2, Mécanique, Physique, Chimie, Sciences de l'univers, Sciences de la Terre*, *300*, 863–868.

15252027, 2023, 6, Downloaded from https://agupubs.onlinelibrary.wiley.com/doi/10.1029/2022GC010843 by Thorsten Becker - University Of Texas Libraries , Wiley Online Library on [12/06/2023]. See the Terms and Conditions (https://onlinelibrary.wiley.com/terms-and-conditions) on Wiley Online Library for rules of use; OA articles are governed by the applicable Creative Commons License

Bezada, M. J., Humphreys, E. D., Davila, J. M., Carbonell, R., Harnafi, M., Palomeras, I., & Levander, A. (2014). Piecewise delamination of Moroccan lithosphere from beneath the Atlas mountains. *Geochemistry, Geophysics, Geosystems*, *15*(4), 975–985. https://doi.org/10.1002/2013gc005059

Bird, P. (1979). Continental delamination and the Colorado Plateau. *Journal of Geophysical Research*, *84*(B13), 7561–7571. https://doi.org/10.1029/jb084ib13p07561

Bondi, M., Morten, L., Nimis, P., Rossi, P. L., & Tranne, C. A. (2002). Megacrysts and mafic–ultramafic xenolith-bearing ignimbrites from Sirwa Volcano, Morocco: Phase petrology and thermobarometry. *Mineralogy and Petrology*, *75*(3–4), 203–221. https://doi.org/10.1007/s007100200024

Bonvalot, S., Balmino, G., Briais, A., Kuhn, M., Peyrefitte, A., Vales, N., et al. (2012). *World gravity map*. Commission for the Geological Map of the World.

Bosch, D., Maury, R. C., Bollinger, C., Bellon, H., & Verdoux, P. (2014). Lithospheric origin for neogene–quaternary middle Atlas lavas (Morocco): Clues from trace elements and Sr–Nd–Pb–Hf isotopes. *Lithos*, *205*, 247–265. https://doi.org/10.1016/j.lithos.2014.07.009

Boulton, S. J., Stokes, M., & Mather, A. E. (2014). Transient fluvial incision as an indicator of active faulting and Plio-Quaternary uplift of the Moroccan high Atlas. *Tectonophysics*, *633*, 16–33. https://doi.org/10.1016/j.tecto.2014.06.032

Brey, G., & Green, D. H. (1977). Systematic study of liquidas phase relations in olivine melilitite + H_2O + CO_2 at high pressures and petrogenesis of an olivine melilitite magma. *Contributions to Mineralogy and Petrology*, *61*(2), 141–162. https://doi.org/10.1007/bf00374364

Burov, E., Guillou-Frottier, L., d'Acremont, E., Le Pourhiet, L., & Cloetingh, S. (2007). Plume head–lithosphere interactions near intra-continental plate boundaries. *Tectonophysics*, *434*(1–4), 15–38. https://doi.org/10.1016/j.tecto.2007.01.002

Calvín, P., Casas-sainz, A. M., Villalaín, J. J., & Moussaid, B. (2018). Tectonophysics extensional vs. compressional deformation in the Central high Atlas salt province: A paleomagnetic approach. *Tectonophysics*, *734–735*, 130–147. https://doi.org/10.1016/j.tecto.2018.04.007

Carracedo, J. C., Badiola, E. R., Guillou, H., de La Nuez, J., & Torrado, F. P. (2001). Geology and volcanology of la Palma and el Hierro, western Canaries. *Estudios Geologicos-Madrid*, *57*, 175–273.

Casalini, M., Tommasini, S., Guarnieri, L., Avanzinelli, R., Lanari, R., Mattei, M., & Conticelli, S. (2022). Subduction-related lamproitic signature in intraplate-like volcanic rocks: The case study of the Tallante alkali basalts, Betic Chain, South-eastern Spain. *Italian Journal of Geosciences*, *141*(1), 144–159. https://doi.org/10.3301/ijg.2022.06

Chamboredon, R. (2015). *Caractérisation et origine des magmas alcalins et des fluides sous le massif volcanique du Jbel Saghro, Anti Atlas*. Maroc.

Chanouan, L., Ikenne, M., Gahlan, H. A., Arai, S., & Youbi, N. (2017). Petrological characteristics of mantle xenoliths from the Azrou-Timahdite quaternary basalts, middle atlas, Morocco: A mineral chemistry perspective. *Journal of African Earth Sciences*, *127*, 235–252. https://doi.org/10.1016/j.jafrearsci.2016.09.004

Charton, R., Bertotti, G., Duval Arnould, A., Storms, J. E. A., & Redfern, J. (2020). Low-temperature thermochronology as a control on vertical movements for semi-quantitative source-to-sink analysis: A case study for the Permian to Neogene of Morocco and surroundings. *Basin Research*, *33*(2), 1337–1383. https://doi.org/10.1111/bre.12517

Choubert, G., Charlot, R., Faure-Muret, A., Hottinger, L., Marcais, J., Tisserant, D., & Vidal, P. (1968). Note préliminaire sur le volcanisme messinien-(pontien) au Maroc. *Comptes rendus de l'Académie des Sciences*, *266*, 197–199.

Civiero, C., Custódio, S., Duarte, J. C., Mendes, V. B., & Faccenna, C. (2020). Dynamics of the Gibraltar arc system: A complex interaction between plate convergence, slab pull, and mantle flow. *Journal of Geophysical Research: Solid Earth*, *125*(7), e2019JB018873. https://doi.org/10.1029/2019jb018873

Civiero, C., Strak, V., Custódio, S., Silveira, G., Rawlinson, N., Arroucau, P., & Corela, C. (2018). A common deep source for upper-mantle upwellings below the Ibero-western Maghreb region from teleseismic P-wave travel-time tomography. *Earth and Planetary Science Letters*, *499*, 157–172. https://doi.org/10.1016/j.epsl.2018.07.024

Clementucci, R., Ballato, P., Siame, L., Fox, M., Lanari, R., Sembroni, A., et al. (2023a). Surface uplift and topographic rejuvenation of a tectonically inactive range: Insights from the Anti-Atlas and the Siroua Massif (Morocco). *Tectonics*, *42*(2), e2022TC007383. https://doi.org/10.1029/2022tc007383

Clementucci, R., Ballato, P., Siame, L. L., Faccenna, C., Racano, S., Torreti, G., et al. (2023b). Transient response to changes in uplift rates in the northern Atlas-Meseta system (Morocco). *Geomorphology*, *435*. https://doi.org/10.2139/ssrn.4263924

Clementucci, R., Ballato, P., Siame, L. L., Faccenna, C., Yaaqoub, A., Essaifi, A., et al. (2022). Lithological control on topographic relief evolution in a slow tectonic setting (Anti-Atlas, Morocco). *Earth and Planetary Science Letters*, *596*, 117788. https://doi.org/10.1016/j.epsl.2022.117788

Clevenger, T. C., & Heister, T. (2021). Comparison between algebraic and matrix-free geometric multigrid for a Stokes problem on adaptive meshes with variable viscosity. *Numerical Linear Algebra with Applications*, *28*(5), e2375. https://doi.org/10.1002/nla.2375

Cloos, M., & Shreve, R. L. (1988). Subduction-channel model of prism accretion, melange formation, sediment subduction, and subduction erosion at convergent plate margins: 2. Implications and discussion. *Pure and Applied Geophysics*, *128*(3–4), 501–545. https://doi.org/10.1007/bf00874549

Craig, T. J., Jackson, J. A., Priestley, K., & McKenzie, D. (2011). Earthquake distribution patterns in Africa: Their relationship to variations in lithospheric and geological structure, and their rheological implications. *Geophysical Journal International*, *185*(1), 403–434. https://doi.org/10.1111/j.1365-246x.2011.04950.x

D'Agostino, N., Jackson, J. A., Dramis, F., & Funiciello, R. (2001). Interactions between mantle upwelling, drainage evolution and active normal faulting: An example from the central Apennines (Italy). *Geophysical Journal International*, *147*(2), 475–497. https://doi.org/10.1046/j.1365-246x.2001.00539.x

Dasgupta, R., Hirschmann, M. M., & Smith, N. D. (2007). Partial melting experiments of peridotite + CO_2 at 3 GPa and genesis of alkalic ocean island basalts. *Journal of Petrology*, *48*(11), 2093–2124. https://doi.org/10.1093/petrology/egm053

DeCelles, P. G., Zandt, G., Beck, S. L., Currie, C. A., Ducea, M. N., Kapp, P., et al. (2014). Cyclical orogenic processes in the Cenozoic central Andes. *Geological Society of America Memoir*, *212*, MWR212-22.

Delaloye, M. B. A. M. (1989). Donn es g ochronologiques nouveiles sur le massif volcanique du Siroua (Anti-Atlas, Maroc) (Vol. *9*, pp. 651–656).

Delcaillau, B., Amrhar, M., Namous, M., Laville, E., Pedoja, K., & Dugué, O. (2011). Transpressional tectonics in the Marrakech high Atlas: Insight by the geomorphic evolution of drainage basins. *Geomorphology*, *134*(3–4), 344–362. https://doi.org/10.1016/j.geomorph.2011.07.010

DeMets, C., Iaffaldano, G., & Merkouriev, S. (2015). High-resolution Neogene and quaternary estimates of Nubia-Eurasia-North America plate motion. *Geophysical Journal International*, *203*(1), 416–427. https://doi.org/10.1093/gji/ggv277

Dewey, J. F., Helman, M. L., Knott, S. D., Turco, E., & Hutton, D. H. W. (1989). Kinematics of the western Mediterranean. *Geological Society, London, Special Publications*, *45*(1), 265–283. https://doi.org/10.1144/gsl.sp.1989.045.01.15

Diaz, J., Gallart, J., & Carbonell, R. (2016). Moho topography beneath the Iberian-Western Mediterranean region mapped from controlled-source and natural seismicity surveys. *Tectonophysics*, *692*, 74–85. https://doi.org/10.1016/j.tecto.2016.08.023

15252027, 2023, 6, Downloaded from https://agupubs.onlinelibrary.wiley.com/doi/10.1029/2022GC010843 by Thorsten Becker - University Of Texas Libraries , Wiley Online Library on [12/06/2023]. See the Terms and Conditions (https://onlinelibrary.wiley.com/terms-and-conditions) on Wiley Online Library for rules of use; OA articles are governed by the applicable Creative Commons License

Díaz, J., Gil, A., Carbonell, R., Gallart, J., & Harnafi, M. (2016). Constraining the crustal root geometry beneath Northern Morocco. *Tectonophysics*, *689*, 14–24. https://doi.org/10.1016/j.tecto.2015.12.009

Domènech, M. (2015). *Rift opening and inversion in the marrakech high Atlas: Integrated structural and thermochronologic study. Ph.D. Thesis* (pp. 1–157). Universitat Autonoma de Barcelona.

Domènech, M., Stockli, D. F., & Teixell, A. (2018). Detrital zircon U–Pb provenance and palaeogeography of Triassic rift basins in the Marrakech High Atlas. *Terra Nova*, *30*(4), 310–318. https://doi.org/10.1111/ter.12340

Domènech, M., Teixell, A., & Stockli, D. F. (2016). Magnitude of rift-related burial and orogenic contraction in the Marrakech High Atlas revealed by zircon (U-Th)/He thermochronology and thermal modeling. *Tectonics*, *35*(11), 2609–2635. https://doi.org/10.1002/2016tc004283

Duggen, S., Hoernle, K., van den Bogaard, P., & Garbe-Schönberg, D. (2005). Post-collisional transition from subduction-to intraplate-type magmatism in the westernmost Mediterranean: Evidence for continental-edge delamination of subcontinental lithosphere. *Journal of Petrology*, *46*(6), 1155–1201. https://doi.org/10.1093/petrology/egi013

Duggen, S., Hoernle, K. A., Hauff, F., Klügel, A., Bouabdellah, M., & Thirlwall, M. F. (2009). Flow of Canary mantle plume material through a subcontinental lithospheric corridor beneath Africa to the Mediterranean: Reply 30653. https://doi.org/10.1130/G30653Y.1

El Azzouzi, M., Bellon, H., Coutelle, A., & Réhault, J.-P. (2014). Miocene magmatism and tectonics within the Peri-Alboran orogen (western Mediterranean). *Journal of Geodynamics*, *77*, 171–185. https://doi.org/10.1016/j.jog.2014.02.006

El Azzouzi, M., Bellon, H., Maury, R. C., Pique, A., Cotten, J., Griffiths, J. B., et al. (1999). Evolution of the sources of Moroccan volcanism during the Neogene. In *Comptes Rendus de l'Academie des Sciences. Serie 2, Sciences de la Terre et des Planetes* (pp. 95–102).

El Azzouzi, M., Maury, R. C., Bellon, H., Youbi, N., Cotten, J., & Kharbouch, F. (2010). Petrology and K-Ar chronology of the neogene-quaternary middle Atlas basaltic province, Morocco. *Bulletin de la Societe Geologique de France*, *181*(3), 243–257. https://doi.org/10.2113/gssgfbull.181.3.243

Ellero, A., Ottria, G., Malusà, M. G., & Ouanaimi, H. (2012). Structural geological analysis of the high Atlas (Morocco): Evidences of a transpressional fold-thrust belt. In *Tectonics-recent advances*. InTech.

El Messbahi, H., Bodinier, J.-L., Vauchez, A., Dautria, J.-M., Ouali, H., & Garrido, C. J. (2015). Short wavelength lateral variability of lithospheric mantle beneath the Middle Atlas (Morocco) as recorded by mantle xenoliths. *Tectonophysics*, *650*, 34–52. https://doi.org/10.1016/j.tecto.2014.11.020

Faccenna, C., & Becker, T. W. (2020). Topographic expressions of mantle dynamics in the Mediterranean. *Earth-Science Reviews*, *103327*, 103327. https://doi.org/10.1016/j.earscirev.2020.103327

Faccenna, C., Becker, T. W., Holt, A. F., & Brun, J. P. (2021). Mountain building, mantle convection, and supercontinents: Revisited. *Earth and Planetary Science Letters*, *564*, 116905. https://doi.org/10.1016/j.epsl.2021.116905

Faccenna, C., Becker, T. W., Jolivet, L., & Keskin, M. (2013). Mantle convection in the Middle East: Reconciling Afar upwelling, Arabia indentation and Aegean trench rollback. *Earth and Planetary Science Letters*, *375*, 254–269. https://doi.org/10.1016/j.epsl.2013.05.043

Faccenna, C., Oncken, O., Holt, A. F., & Becker, T. W. (2017). Initiation of the Andean orogeny by lower mantle subduction. *Earth and Planetary Science Letters*, *463*, 189–201. https://doi.org/10.1016/j.epsl.2017.01.041

Faccenna, C., Piromallo, C., Crespo-Blanc, A., Jolivet, L., & Rossetti, F. (2004). Lateral slab deformation and the origin of the western Mediterranean arcs. *Tectonics*, *23*(1), TC1012. https://doi.org/10.1029/2002TC001488

Falloon, T. J., & Green, D. H. (1989). The solidus of carbonated, fertile peridotite. *Earth and Planetary Science Letters*, *94*(3–4), 364–370. https://doi.org/10.1016/0012-821x(89)90153-2

Faure, G. (2013). *Origin of igneous rocks: The isotopic evidence*. Springer Science & Business Media.

Fekkak, A., Ouanaimi, H., Michard, A., Soulaimani, A., Ettachfini, E. M., Berrada, I., et al. (2018). Thick-skinned tectonics in a Late Cretaceous-Neogene intracontinental belt (High Atlas Mountains, Morocco): The flat-ramp fault control on basement shortening and cover folding. *Journal of African Earth Sciences*, *140*, 169–188. https://doi.org/10.1016/j.jafrearsci.2018.01.008

Fraters, M., Thieulot, C., Van Den Berg, A., & Spakman, W. (2019). The geodynamic World Builder: A solution for complex initial conditions in numerical modeling. *Solid Earth*, *10*(5), 1785–1807. https://doi.org/10.5194/se-10-1785-2019

Frey, F. A., Green, D. H., & Roy, S. D. (1978). Integrated models of basalt petrogenesis: A study of quartz tholeiites to olivine melilitites from south eastern Australia utilizing geochemical and experimental petrological data. *Journal of Petrology*, *19*(3), 463–513. https://doi.org/10.1093/petrology/19.3.463

Frizon de Lamotte, D., Leturmy, P., Missenard, Y., Khomsi, S., Ruiz, G., Saddiqi, O., et al. (2009). Mesozoic and Cenozoic vertical movements in the Atlas system (Algeria, Morocco, Tunisia): An overview. *Tectonophysics*, *475*(1), 9–28. https://doi.org/10.1016/j.tecto.2008.10.024

Frizon de Lamotte, D., Saint Bezar, B., Bracène, R., & Mercier, E. (2000). The two main steps of the Atlas building and geodynamics of the western Mediterranean. *Tectonics*, *19*(4), 740–761. https://doi.org/10.1029/2000tc900003

Fullea, J., Fernàndez, M., Afonso, J. C., Vergés, J., & Zeyen, H. (2010). The structure and evolution of the lithosphere-asthenosphere boundary beneath the Atlantic-Mediterranean Transition Region. *Lithos*, *120*(1–2), 74–95. https://doi.org/10.1016/j.lithos.2010.03.003

Funiciello, F., Moroni, M., Piromallo, C., Faccenna, C., Cenedese, A., & Bui, H. A. (2006). Mapping mantle flow during retreating subduction: Laboratory models analyzed by feature tracking. *Journal of Geophysical Research*, *111*(B3), 1–16. https://doi.org/10.1029/2005JB003792

Ghorbal, B. (2009). Mesozoic to Quaternary thermo-tectonic evolution of Morocco (NW Africa).

Ghorbal, B., Bertotti, G., Foeken, J., & Andriessen, P. (2008). Unexpected Jurassic to Neogene vertical movements in 'stable' parts of NW Africa revealed by low temperature geochronology. *Terra Nova*, *20*(5), 355–363. https://doi.org/10.1111/j.1365-3121.2008.00828.x

Gleason, G. C., & Tullis, J. (1995). A flow law for dislocation creep of quartz aggregates determined with the molten salt cell. *Tectonophysics*, *247*(1–4), 1–23. https://doi.org/10.1016/0040-1951(95)00011-b

Glerum, A., Thieulot, C., Fraters, M., Blom, C., & Spakman, W. (2018). Nonlinear viscoplasticity in ASPECT: Benchmarking and applications to subduction. *Solid Earth*, *9*(2), 267–294. https://doi.org/10.5194/se-9-267-2018

Göğüş, O. H. (2020). Geodynamic experiments suggest that mantle plume caused Late Permian Emeishan Large Igneous Province in Southern China. *International Geology Review*, *64*(3), 1–15. https://doi.org/10.1080/00206814.2020.1855602

Göğüş, O. H., & Psyklywec, R. N. (2008). Mantle lithosphere delamination driving plateau uplift and synconvergent extension in eastern Anatolia. *Geology*, *36*, 723–726. https://doi.org/10.1130/G24982A.1

Göğüş, O. H., & Ueda, K. (2018). Peeling back the lithosphere: Controlling parameters, surface expressions and the future directions in delamination modeling. *Journal of Geodynamics*, *117*, 21–40. https://doi.org/10.1016/j.jog.2018.03.003

Gomez, F., Allmendinger, R., Barazangi, M., Er-Raji, A., & Dahmani, M. (1998). Crustal shortening and vertical strain partitioning in the Middle Atlas Mountains of Morocco. *Tectonics*, *17*(4), 520–533. https://doi.org/10.1029/98tc01439

Gomez, F., Beauchamp, W., & Barazangi, M. (2000). Role of the Atlas mountains (northwest Africa) within the African-Eurasian plate-boundary zone. *Geology*, *28*(9), 775–778. https://doi.org/10.1130/0091-7613(2000)28<775:rotamn>2.0.co;2

15252027, 2023, 6, Downloaded from https://agupubs.onlinelibrary.wiley.com/doi/10.1029/2022GC010843 by Thorsten Becker - University Of Texas Libraries , Wiley Online Library on [12/06/2023]. See the Terms and Conditions (https://onlinelibrary.wiley.com/terms-and-conditions) on Wiley Online Library for rules of use; OA articles are governed by the applicable Creative Commons License

Gómez-Ulla, A., Sigmarsson, O., Huertas, M. J., Devidal, J. L., & Ancochea, E. (2018). The historical basanite-alkali basalt-tholeiite suite at Lanzarote, Canary Islands: Carbonated melts of heterogeneous mantle source? *Chemical Geology*, *494*, 56–68. https://doi.org/10.1016/j.chemgeo.2018.07.015

Gouiza, M., Charton, R., Bertotti, G., Andriessen, P., & Storms, J. E. A. (2017). Post-Variscan evolution of the Anti-Atlas belt of Morocco constrained from low-temperature geochronology. *International Journal of Earth Sciences*, *106*(2), 593–616. https://doi.org/10.1007/s00531-016-1325-0

Gudfinnsson, G. H., & Presnall, D. C. (2005). Continuous gradations among primary carbonatitic, kimberlitic, melilititic, basaltic, picritic, and komatiitic melts in equilibrium with garnet lherzolite at 3–8 GPa. *Journal of Petrology*, *46*(8), 1645–1659. https://doi.org/10.1093/petrology/egi029

Guimerà, J., Arboleya, M. L., & Teixell, A. (2011). Structural control on present-day topography of a basement massif: The central and Eastern anti-atlas (Morocco). *Geológica Acta*, *9*, 55–65. https://doi.org/10.1344/105.000001643

Gurenko, A. A., Hoernle, K. A., Hauff, F., Schmincke, H. U., Han, D., Miura, Y. N., & Kaneoka, I. (2006). Major, trace element and Nd–Sr–Pb–O–He–Ar isotope signatures of shield stage lavas from the central and western Canary Islands: Insights into mantle and crustal processes. *Chemical Geology*, *233*(1–2), 75–112. https://doi.org/10.1016/j.chemgeo.2006.02.016

Gurnis, M., Mitrovica, J. X., Ritsema, J., & van Heijst, H. (2000). Constraining mantle density structure using geological evidence of surface uplift rates: The case of the African superplume. *Geochemistry, Geophysics, Geosystems*, *1*(7), GC000035. https://doi.org/10.1029/1999gc000035

He, Y., Puckett, E. G., & Billen, M. I. (2017). A discontinuous Galerkin method with a bound preserving limiter for the advection of non-diffusive fields in solid Earth geodynamics. *Physics of the Earth and Planetary Interiors*, *263*, 23–37. https://doi.org/10.1016/j.pepi.2016.12.001

Heister, T., Dannberg, J., Gassmöller, R., & Bangerth, W. (2017). High accuracy mantle convection simulation through modern numerical methods-II: Realistic models and problems. *Geophysical Journal International*, *210*(2), 833–851. https://doi.org/10.1093/gji/ggx195

Hirose, K. (1997). Melting experiments on lherzolite KLB-1 under hydrous conditions and generation of high-magnesian andesitic melts. *Geology*, *25*(1), 42–44. https://doi.org/10.1130/0091-7613(1997)025<0042:meolku>2.3.co;2

Hirth, G., & Kohlstedt, D. L. (1996). Water in the oceanic upper mantle: Implications for rheology, melt extraction and the evolution of the lithosphere. *Earth and Planetary Science Letters*, *144*(1–2), 93–108. https://doi.org/10.1016/0012-821x(96)00154-9

Hoernle, K. A. J., Zhang, Y.-S., & Graham, D. (1995). Seismic and geochemical evidence for large-scale mantle upwelling beneath the eastern Atlantic and western and central Europe. *Nature*, *374*(6517), 34–39. https://doi.org/10.1038/374034a0

Hofmann, A. W. (1997). Mantle geochemistry: The message from oceanic volcanism. *Nature*, *385*(6613), 219–229. https://doi.org/10.1038/385219a0

Hssaine, A. A., & Bridgland, D. (2009). Pliocene–Quaternary fluvial and aeolian records in the Souss Basin, southwest Morocco: A geomorphological model. *Global and Planetary Change*, *68*(4), 288–296. https://doi.org/10.1016/j.gloplacha.2009.03.002

Ibhi, A., & Nachit, H. (2000). The substitution mechanism of Ba and Ti into phyllosilicate phases: The example of barium-titanium biotite. In *Annales de Chimie Science des Matériaux* (Vol. 25, pp. 627–634). Elsevier.

Isacks, B., Oliver, J., & Sykes, L. R. (1968). Seismology and the new global tectonics. *Journal of Geophysical Research*, *73*(18), 5855–5899. https://doi.org/10.1029/jb073i018p05855

Jung, S., & Hellebrand, E. (2006). Trace element fractionation during high-grade metamorphism and crustal melting—Constraints from ion microprobe data of metapelitic, migmatitic and igneous garnets and implications for Sm–Nd garnet chronology. *Lithos*, *87*(3–4), 193–213. https://doi.org/10.1016/j.lithos.2005.06.013

Kaus, B. J. P., Mühlhaus, H., & May, D. A. (2010). A stabilization algorithm for geodynamic numerical simulations with a free surface. *Physics of the Earth and Planetary Interiors*, *181*(1–2), 12–20. https://doi.org/10.1016/j.pepi.2010.04.007

Kincaid, C., Druken, K. A., Griffiths, R. W., & Stegman, D. R. (2013). Bifurcation of the Yellowstone plume driven by subduction-induced mantle flow. *Nature Geoscience*, *6*(5), 395–399. https://doi.org/10.1038/ngeo1774

Klemme, S., & O'Neill, H. S. (2000). The near-solidus transition from garnet lherzolite to spinel lherzolite. *Contributions to Mineralogy and Petrology*, *138*(3), 237–248. https://doi.org/10.1007/s004100050560

Krijgsman, W., Langereis, C. G., Zachariasse, W. J., Boccaletti, M., Moratti, G., Gelati, R., et al. (1999). Late Neogene evolution of the Taza–Guercif Basin (Rifian Corridor, Morocco) and implications for the Messinian salinity crisis. *Marine Geology*, *153*(1–4), 147–160. https://doi.org/10.1016/s0025-3227(98)00084-x

Kronbichler, M., Heister, T., & Bangerth, W. (2012). High accuracy mantle convection simulation through modern numerical methods. *Geophysical Journal International*, *191*(1), 12–29. https://doi.org/10.1111/j.1365-246x.2012.05609.x

Kurzweil, F., Muenker, C., Grupp, M., Braukmüller, N., Fechtner, L., Christian, M., et al. (2019). The stable tungsten isotope composition of modern igneous reservoirs. *Geochimica et Cosmochimica Acta*, *251*, 176–191. https://doi.org/10.1016/j.gca.2019.02.025

Kushiro, I. (1975). Carbonate-silicate reactions at high pressures and possible presence of dolomite and magnesite in the upper mantle. *Earth and Planetary Science Letters*, *28*(2), 116–120. https://doi.org/10.1016/0012-821x(75)90218-6

Lanari, R. (2023). Miocene mantle dynamics and intraplate orogeny: The Atlas of Morocco [Dataset]. OSF. Retrieved from https://osf.io/mwcbq/

Lanari, R., Boutoux, A., Faccenna, C., Herman, F., Willett, S. D., & Ballato, P. (2023). Cenozoic exhumation in the Mediterranean and the Middle East. *Earth-Science Reviews*, *237*, 104328. https://doi.org/10.1016/j.earscirev.2023.104328

Lanari, R., Faccenna, C., Fellin, M. G., Abderrahim, E., Nahid, A., Medina, F., & Youbi, N. (2020a). Tectonic evolution of the Western high Atlas of Morocco: Oblique convergence, reactivation and transpression. *Tectonics*, *39*(3), e2019TC005563. https://doi.org/10.1029/2019tc005563

Lanari, R., Fellin, M. G., Faccenna, C., Balestrieri, M. L., Pazzaglia, F., Youbi, N., & Maden, C. (2020b). Exhumation and surface evolution of the Western High-Atlas and surrounding regions as constrained by low-temperature thermochronology. *Tectonics*, *39*(3), e2019TC005562. https://doi.org/10.1029/2019tc005562

Lanari, R., Reitano, R., Faccenna, C., Agostinetti, N. P., & Ballato, P. (2023). Surface and crustal response to deep subduction dynamics: Insight from the Apennines, Italy. *Tectonics*, *42*, e2022TC007461. https://doi.org/10.1029/2022TC007461

Lanari, R., Reitano, R., Giachetta, E., Pazzaglia, F. J., Clementucci, R., Faccenna, C., & Fellin, M. G. (2022). Is the Anti-Atlas of Morocco still uplifting? *Journal of African Earth Sciences*, *188*, 104481. https://doi.org/10.1016/j.jafrearsci.2022.104481

Laske, G., Masters, G., Ma, Z., & Pasyanos, M. (2013). Update on CRUST1.0—A 1-degree global model of Earth's crust. In *Geophysical research abstracts EGU general assembly* (p. 2658).

Leprêtre, R., Missenard, Y., Barbarand, J., Gautheron, C., Jouvie, I., & Saddiqi, O. (2018). Polyphased inversions of an intracontinental rift: Case study of the Marrakech high Atlas, Morocco. *Tectonics*, *37*(3), 818–841. https://doi.org/10.1002/2017tc004693

Leprêtre, R., Missenard, Y., Saint-Bezar, B., Barbarand, J., Delpech, G., Yans, J., et al. (2015). The three main steps of the Marrakech High Atlas building in Morocco: Structural evidences from the southern foreland, Imini area. *Journal of African Earth Sciences*, *109*, 177–194. https://doi.org/10.1016/j.jafrearsci.2015.05.013

15252027, 2023, 6, Downloaded from https://agupubs.onlinelibrary.wiley.com/doi/10.1029/2022GC010843 by Thorsten Becker - University Of Texas Libraries , Wiley Online Library on [12/06/2023]. See the Terms and Conditions (https://onlinelibrary.wiley.com/terms-and-conditions) on Wiley Online Library for rules of use; OA articles are governed by the applicable Creative Commons License

Lucassen, F., Franz, G., Romer, R. L., Pudlo, D., & Dulski, P. (2008). Nd, Pb, and Sr isotope composition of Late Mesozoic to quaternary intra-plate magmatism in NE-Africa (Sudan, Egypt): High-μ signatures from the mantle lithosphere. *Contributions to Mineralogy and Petrology*, *156*(6), 765–784. https://doi.org/10.1007/s00410-008-0314-0

Lundstrom, C. C., Hoernle, K., & Gill, J. (2003). U-series disequilibria in volcanic rocks from the Canary Islands: Plume versus lithospheric melting. *Geochimica et Cosmochimica Acta*, *67*(21), 4153–4177. https://doi.org/10.1016/s0016-7037(03)00308-9

Lustrino, M., & Wilson, M. (2007). The circum-Mediterranean anorogenic Cenozoic igneous province. *Earth-Science Reviews*, *81*(1–2), 1–65. https://doi.org/10.1016/j.earscirev.2006.09.002

Makris, J., Demnati, A., & Klussmann, J. (1985). Deep seismic soundings in Morocco and a crust and upper mantle model deduced from seismic and gravity data. In *Annales de Géophysique* (pp. 369–380).

Malarkey, J., Wittig, N., Graham Pearson, D., & Davidson, J. P. (2011). Characterising modal metasomatic processes in young continental lithospheric mantle: A microsampling isotopic and trace element study on xenoliths from the middle Atlas mountains, Morocco. *Contributions to Mineralogy and Petrology*, *162*(2), 289–302. https://doi.org/10.1007/s00410-010-0597-9

Malusà, M. G., Polino, R., Feroni, A. C., Ellero, A., Ottria, G., Baidder, L., & Musumeci, G. (2007). Post-Variscan tectonics in eastern anti-atlas (Morocco). *Terra Nova*, *19*(6), 481–489. https://doi.org/10.1111/j.1365-3121.2007.00775.x

Mancilla, F. D. L., & Diaz, J. (2015). High resolution Moho topography map beneath Iberia and Northern Morocco from receiver function analysis. *Tectonophysics*, *663*, 203–211. https://doi.org/10.1016/j.tecto.2015.06.017

Martí, J., Castro, A., Rodríguez, C., Costa, F., Carrasquilla, S., Pedreira, R., & Bolos, X. (2013). Correlation of magma evolution and geophysical monitoring during the 2011–2012 El Hierro (Canary Islands) submarine eruption. *Journal of Petrology*, *54*(7), 1349–1373. https://doi.org/10.1093/petrology/egt014

Mattei, M., Riggs, N. R., Giordano, G., Guarnieri, L., Cifelli, F., Soriano, C. C., et al. (2014). Geochronology, geochemistry and geodynamics of the Cabo de Gata volcanic zone, Southeastern Spain. *Italian Journal of Geosciences*, *133*(3), 341–361. https://doi.org/10.3301/ijg.2014.44

Maza, M., Briqueu, L., Dautria, J.-M., & Bosch, D. (1998). Le complexe annulaire d'age Oligocene de l'Achkal (Hoggar central, Sud Algerie): Temoin de la transition au cenozoique entre les magmatismes tholeitique et alcalin. Evidences par les isotopes du Sr, Nd et Pb. *Comptes Rendus de l'Academie des Sciences - Series IIA: Earth and Planetary Science*, *327*(3), 167–172. https://doi.org/10.1016/s1251-8050(98)80004-9

McKenzie, D., & Fairhead, D. (1997). Estimates of the effective elastic thickness of the continental lithosphere from Bouguer and free air gravity anomalies. *Journal of Geophysical Research*, *102*(B12), 27523–27552. https://doi.org/10.1029/97jb02481

Meghraoui, M., Outtani, F., Choukri, A., & De Lamotte, D. F. (1999). Coastal tectonics across the South Atlas thrust front and the Agadir active zone, Morocco. *Geological Society, London, Special Publications*, *146*(1), 239–253. https://doi.org/10.1144/gsl.sp.1999.146.01.14

Memiş, C., Göğüş, O. H., Uluocak, S. E., Pysklywec, R., Keskin, M., Şengör, A. M. C., & Topuz, G. (2020). Long wavelength progressive plateau uplift in eastern Anatolia since 20 Ma: Implications for the role of slab peel back and break off. *Geochemistry, Geophysics, Geosystems*, *212*, e2019GC008726. https://doi.org/10.1029/2019GC008726

Mengel, K., & Green, D. H. (1986). Experimental study of amphibole and phlogopite stability in metasomatized peridotite under water-saturated and water-undersaturated conditions. In *International Kimberlite conference: Extended abstracts* (pp. 193–195).

Mériaux, C. A., Duarte, J. C., Duarte, S. S., Schellart, W. P., Chen, Z., Rosas, F., et al. (2015). Capture of the Canary mantle plume material by the Gibraltar arc mantle wedge during slab rollback. *Geophysical Journal International*, *201*(3), 1717–1721. https://doi.org/10.1093/gji/ggv120

Miller, M. S., & Becker, T. W. (2014). Reactivated lithospheric-scale discontinuities localize dynamic uplift of the Moroccan Atlas Mountains. *Geology*, *42*(1), 35–38. https://doi.org/10.1130/G34959.1

Miller, M. S., O'Driscoll, L. J., Butcher, A. J., & Thomas, C. (2015). Imaging Canary Island hotspot material beneath the lithosphere of Morocco and southern Spain. *Earth and Planetary Science Letters*, *431*, 186–194. https://doi.org/10.1016/j.epsl.2015.09.026

Missenard, Y., & Cadoux, A. (2012). Can Moroccan Atlas lithospheric thinning and volcanism be induced by Edge-Driven Convection? *Terra Nova*, *24*(1), 27–33. https://doi.org/10.1111/j.1365-3121.2011.01033.x

Missenard, Y., Saddiqi, O., Barbarand, J., Leturmy, P., Ruiz, G., El Haimer, F. Z., & de Lamotte, D. F. (2008). Cenozoic denudation in the Marrakech high Atlas, Morocco: Insight from apatite fission-track thermochronology. *Terra Nova*, *20*(3), 221–228. https://doi.org/10.1111/j.1365-3121.2008.00810.x

Missenard, Y., Taki, Z., Frizon de Lamotte, D., Benammi, M., Hafid, M., Leturmy, P., & Sébrier, M. (2007). Tectonic styles in the Marrakesh High Atlas (Morocco): The role of heritage and mechanical stratigraphy. *Journal of African Earth Sciences*, *48*(4), 247–266. https://doi.org/10.1016/j.jafrearsci.2007.03.007

Missenard, Y., Zeyen, H., de Lamotte, D. F., Leturmy, P., Petit, C., Sébrier, M., & Saddiqi, O. (2006). Crustal versus asthenospheric origin of relief of the Atlas mountains of Morocco. *Journal of Geophysical Research*, *111*, 1–13. https://doi.org/10.1029/2005JB003708

Molin, P., Fubelli, G., Nocentini, M., Sperini, S., Ignat, P., Grecu, F., & Dramis, F. (2012). Interaction of mantle dynamics, crustal tectonics, and surface processes in the topography of the Romanian Carpathians: A geomorphological approach. *Global and Planetary Change*, *90*(91), 58–72. https://doi.org/10.1016/j.gloplacha.2011.05.005

Molnar, P., & Houseman, G. A. (2015). Effects of a low-viscosity lower crust on topography and gravity at convergent mountain belts during gravitational instability of mantle lithosphere. *Journal of Geophysical Research: Solid Earth*, *120*(1), 537–551. https://doi.org/10.1002/2014jb011349

Mysen, B. O., & Kushiro, I. (1977). Compositional variations of coexisting phases with degree of melting of peridotite in the upper mantle. *American Mineralogist*, *62*, 843–856.

Naliboff, J., & Buiter, S. J. (2015). Rift reactivation and migration during multiphase extension. *Earth and Planetary Science Letters*, *421*, 58–67. https://doi.org/10.1016/j.epsl.2015.03.050

Natali, C., Beccaluva, L., Bianchini, G., Ellam, R. M., Siena, F., & Stuart, F. M. (2013). Carbonated alkali-silicate metasomatism in the North Africa lithosphere: Evidence from middle Atlas spinel-lherzolites, Morocco. *J South Am Earth Sci*, *41*, 113–121. https://doi.org/10.1016/j.jsames.2012.06.014

Oukassou, M., Saddiqi, O., Barbarand, J., Sebti, S., Baidder, L., & Michard, A. (2013). Post-Variscan exhumation of the Central Anti-Atlas (Morocco) constrained by zircon and apatite fission-track thermochronology. *Terra Nova*, *25*(2), 151–159. https://doi.org/10.1111/ter.12019

Oyarzun, R., Doblas, M., López-Ruiz, J., & María Cebrá, J. (1997). Opening of the central Atlantic and asymmetric mantle upwelling phenomena: Implications for long-lived magmatism in western North Africa and Europe. *Geology*, *25*(8), 727–730. https://doi.org/10.1130/0091-7613(1997)025<0727:ootcaa>2.3.co;2

Palomeras, I., Thurner, S., Levander, A., Liu, K., Villasenor, A., Carbonell, R., & Harnafi, M. (2014). Finite-frequency Rayleigh wave tomography of the western Mediterranean: Mapping its lithospheric structure. *Geochemistry, Geophysics, Geosystems*, *15*(1), 140–160. https://doi.org/10.1002/2013GC004861

Palomeras, I., Villaseñor, A., Thurner, S., Levander, A., Gallart, J., & Harnafi, M. (2017). Lithospheric structure of Iberia and Morocco using finite-frequency Rayleigh wave tomography from earthquakes and seismic ambient noise. *Geochemistry, Geophysics, Geosystems*, *18*(5), 1824–1840. https://doi.org/10.1002/2016gc006657

15252027, 2023, 6, Downloaded from https://agupubs.onlinelibrary.wiley.com/doi/10.1029/2022GC010843 by Thorsten Becker - University Of Texas Libraries , Wiley Online Library on [12/06/2023]. See the Terms and Conditions (https://onlinelibrary.wiley.com/terms-and-conditions) on Wiley Online Library for rules of use; OA articles are governed by the applicable Creative Commons License

Parat, F., Holtz, F., & Klügel, A. (2011). S-rich apatite-hosted glass inclusions in xenoliths from La Palma: Constraints on the volatile partitioning in evolved alkaline magmas. *Contributions to Mineralogy and Petrology*, *162*(3), 463–478. https://doi.org/10.1007/s00410-011-0606-7

Pastor, A., Babault, J., Owen, L. A., Teixell, A., & Arboleya, M. L. (2015). Extracting dynamic topography from river profiles and cosmogenic nuclide geochronology in the Middle Atlas and the High Plateaus of Morocco. *Tectonophysics*, *663*, 95–109. https://doi.org/10.1016/j.tecto.2015.06.007

Pastor, A., Babault, J., Teixell, A., & Arboleya, M. L. (2012). Intrinsic stream-capture control of stepped fan pediments in the High Atlas piedmont of Ouarzazate (Morocco). *Geomorphology*, *173–174*, 88–103. https://doi.org/10.1016/j.geomorph.2012.05.032

Pérez-Gussinyé, M., Lowry, A. R., & Watts, A. B. (2007). Effective elastic thickness of South America and its implications for intracontinental deformation. Geochemistry, Geophysics. *Geosystems*, *8*(5), Q05009. https://doi.org/10.1029/2006GC001511

Platt, J. P., & Vissers, R. L. M. (1989). Extensional collapse of thickened continental lithosphere: A working hypothesis for the Alboran Sea and Gibraltar arc. *Geology*, *17*(6), 540–543. https://doi.org/10.1130/0091-7613(1989)017<0540:ecotcl>2.3.co;2

Prægel, N. O., & Holm, P. M. (2006). Lithospheric contributions to high-MgO basanites from the Cumbre Vieja Volcano, La Palma, Canary Islands and evidence for temporal variation in plume influence. *Journal of Volcanology and Geothermal Research*, *149*(3–4), 213–239. https://doi.org/10.1016/j.jvolgeores.2005.07.019

Raffone, N., Chazot, G., Pin, C., Vannucci, R., & Zanetti, A. (2009). Metasomatism in the lithospheric mantle beneath Middle Atlas (Morocco) and the origin of Fe-and Mg-rich wehrlites. *Journal of Petrology*, *50*(2), 197–249. https://doi.org/10.1093/petrology/egn069

Ramdani, F. (1998). Geodynamic implications of intermediate-depth earthquakes and volcanism in the intraplate Atlas Mountains (Morocco). *Physics of the Earth and Planetary Interiors*, *108*(3), 245–260. https://doi.org/10.1016/S0031-9201(98)00106-X

Ranalli, G. (1995). *Rheology of the Earth*. Springer Science & Business Media.

Robinson, J. A. C., & Wood, B. J. (1998). The depth of the spinel to garnet transition at the peridotite solidus. *Earth and Planetary Science Letters*, *164*(1–2), 277–284. https://doi.org/10.1016/s0012-821x(98)00213-1

Rose, I., Buffett, B., & Heister, T. (2017). Stability and accuracy of free surface time integration in viscous flows. *Physics of the Earth and Planetary Interiors*, *262*, 90–100. https://doi.org/10.1016/j.pepi.2016.11.007

Roy, M., Jordan, T. H., & Pederson, J. (2009). Colorado Plateau magmatism and uplift by warming of heterogeneous lithosphere. *Nature*, *459*(7249), 978–982. https://doi.org/10.1038/nature08052

Royden, L., & Faccenna, C. (2018). Subduction orogeny and the Late Cenozoic evolution of the Mediterranean Arcs. *Annual Review of Earth and Planetary Sciences*, *46*(1), 261–289. https://doi.org/10.1146/annurev-earth-060115-012419

Ruiz, G. M. H., Sebti, S., Negro, F., Saddiqi, O., Frizon de Lamotte, D., Stockli, D., et al. (2011). From central Atlantic continental rift to Neogene uplift–western Anti-Atlas (Morocco). *Terra Nova*, *23*(1), 35–41. https://doi.org/10.1111/j.1365-3121.2010.00980.x

Russo, R. M., & Silver, P. G. (1996). Cordillera formation, mantle dynamics, and the Wilson cycle. *Geology*, *24*(6), 511–514. https://doi.org/10.1130/0091-7613(1996)024<0511:cfmdat>2.3.co;2

Seber, D., Barazangi, M., Tadili, B. A., Ramdani, M., Ibenbrahim, A., Sari, D. B., & Ben Sari, D. (1996). Three-dimensional upper mantle structure beneath the intraplate Atlas and interplate Rif mountains of Morocco. *Journal of Geophysical Research*, *101*(B2), 3125–3138. https://doi.org/10.1029/95JB03112

Sébrier, M., Siame, L., Zouine, E. M., Winter, T., Missenard, Y., & Leturmy, P. (2006). Active tectonics in the Moroccan high Atlas. *Comptes Rendus Geoscience*, *338*(1–2), 65–79. https://doi.org/10.1016/j.crte.2005.12.001

Sebti, S., Saddiqi, O., El Haimer, F. Z., Michard, A., Ruiz, G., Bousquet, R., et al. (2009). Vertical movements at the fringe of the West African Craton: First zircon fission track datings from the Anti-Atlas Precambrian basement, Morocco. *Comptes Rendus Geoscience*, *341*(1), 71–77. https://doi.org/10.1016/j.crte.2008.11.006

Şengül-Uluocak, E., Pysklywec, R. N., Göğüş, O. H., & Ulugergerli, E. U. (2019). Multidimensional geodynamic modeling in the Southeast Carpathians: Upper mantle flow-induced surface topography anomalies. *Geochemistry, Geophysics, Geosystems*, *20*(7), 3134–3149. https://doi.org/10.1029/2019gc008277

Simons, F. J., Zuber, M. T., & Korenaga, J. (2000). Isostatic response of the Australian lithosphere: Estimation of effective elastic thickness and anisotropy using multitaper spectral analysis. *Journal of Geophysical Research*, *105*(B8), 19163–19184. https://doi.org/10.1029/2000jb900157

Skikra, H., Amrouch, K., Soulaimani, A., Leprêtre, R., Ouabid, M., & Bodinier, J. L. (2021). The intracontinental high Atlas belt: Geological overview and pending questions. *Arabian Journal of Geosciences*, *14*(12), 1071. https://doi.org/10.1007/s12517-021-07346-2

Soukrati, A., Youbi, N., Grégoire, M., Berger, J., Boumehdi, M. A., Ibhi, A., & Chaham, K. R. (2021). Pyroxenite xenoliths and clinopyroxene megacrysts from the Cenozoic Jbel Saghro Volcanic field (Anti-Atlas, Morocco): Petrography, mineral chemistry and equilibration conditions. *Geochemistry*, *81*(1), 125694. https://doi.org/10.1016/j.chemer.2020.125694

Soumaya, A., Ben Ayed, N., Rajabi, M., Meghraoui, M., Delvaux, D., Kadri, A., et al. (2018). Active faulting geometry and Stress pattern near complex strike-slip system along the Maghreb region: Constraints on active convergence in the Western Mediterranean. *Tectonics*, *37*(9), 1–26. https://doi.org/10.1029/2018TC004983

Stokes, M., Mather, A. E., Belfoul, M., Faik, F., Bouzid, S., Geach, M. R., et al. (2017). Controls on dryland mountain landscape development along the NW Saharan desert margin: Insights from Quaternary river terrace sequences (Dadès River, south-central High Atlas, Morocco). *Quaternary Science Reviews*, *166*, 363–379. https://doi.org/10.1016/j.quascirev.2017.04.017

Sun, D., Miller, M. S., Holt, A. F., & Becker, T. W. (2014). Hot upwelling conduit beneath the Atlas mountains, Morocco. *Geophysical Research Letters*, *41*(22), 8037–8044. https://doi.org/10.1002/2014GL061884

Sun, S. S., & McDonough, W. F. (1989). Chemical and isotopic systematics of oceanic basalts: Implications for mantle composition and processes. *Geological Society, London, Special Publications*, *42*(1), 313–345. https://doi.org/10.1144/gsl.sp.1989.042.01.19

Tadili, B., Ramdani, M., Ben Sari, D., Chapochnikov, K., & Bellot, A. (1986). Structure de la croûte dans le nord du Maroc. In *Annales geophysicae. Series B. Terrestrial and planetary physics* (pp. 99–104).

Teixell, A., Arboleya, M. L., Julivert, M., & Charroud, M. (2003). Tectonic shortening and topography in the central High Atlas (Morocco). *Tectonics*, *22*(5), 1051. https://doi.org/10.1029/2002TC001460

Teixell, A., Ayarza, P., Zeyen, H., Fernàndez, M., & Arboleya, M. L. (2005). Effects of mantle upwelling in a compressional setting: The Atlas Mountains of Morocco. *Terra Nova*, *17*(5), 456–461. https://doi.org/10.1111/j.1365-3121.2005.00633.x

Teixell, A., Barnolas, A., Rosales, I., & Arboleya, M. (2017). Structural and facies architecture of a diapir-related carbonate minibasin (lower and middle Jurassic, High Atlas, Morocco). *Marine and Petroleum Geology*, *81*, 334–360. https://doi.org/10.1016/j.marpetgeo.2017.01.003

Tesòn, E., & Teixell, A. (2008). Sequence of thrusting and syntectonic sedimentation in the eastern Sub-Atlas thrust belt (Dadès and Mgoun valleys, Morocco). *International Journal of Earth Sciences*, *97*(1), 103–113. https://doi.org/10.1007/s00531-006-0151-1

Thibault, Y., Edgar, A. D., & Lloyd, F. E. (1992). Experimental investigation of melts from a carbonated phlogopite lherzolite: Implications for metasomatism in the continental lithospheric mantle. *American Mineralogist*, *77*, 784–794.

15252027, 2023, 6, Downloaded from https://agupubs.onlinelibrary.wiley.com/doi/10.1029/2022GC010843 by Thorsten Becker - University Of Texas Libraries , Wiley Online Library on [12/06/2023]. See the Terms and Conditions (https://onlinelibrary.wiley.com/terms-and-conditions) on Wiley Online Library for rules of use; OA articles are governed by the applicable Creative Commons License

Thomson, D. J. (1982). Spectrum estimation and harmonic analysis. *Proceedings of the IEEE*, *70*(9), 1055–1096. https://doi.org/10.1109/proc.1982.12433

Turner, S., Hoernle, K., Hauff, F., Johansen, T. S., Klügel, A., Kokfelt, T., & Lundstrom, C. (2015). ^{238}U–^{230}Th–^{226}Ra disequilibria constraints on the magmatic evolution of the Cumbre Vieja volcanics on La Palma, Canary Islands. *Journal of Petrology*, *56*(10), 1999–2024. https://doi.org/10.1093/petrology/egv061

Turner, S. P., Platt, J. P., George, R. M. M., Kelley, S. P., Pearson, D. G., & Nowell, G. M. (1999). Magmatism associated with orogenic collapse of the Betic–Alboran domain, SE Spain. *Journal of Petrology*, *40*(6), 1011–1036. https://doi.org/10.1093/petroj/40.6.1011

Uluocak, E. Ş., Pysklywec, R., & Göğüş, O. H. (2016). Present-day dynamic and residual topography in Central Anatolia. *Geophysical Journal International*, *206*(3), 1515–1525. https://doi.org/10.1093/gji/ggw225

Wang, L. H., Yarushina, V. M., Alkhimenkov, Y., & Podladchikov, Y. (2022). Physics-inspired pseudo-transient method and its application in modelling focused fluid flow with geological complexity. *Geophysical Journal International*, *229*, 1–20. https://doi.org/10.1093/gji/ggab426

Wegmann, K. W., Zurek, B. D., Regalla, C. A., Bilardello, D., Wollenberg, J. L., Kopczynski, S. E., et al. (2007). Position of the snake river watershed divide as an indicator of geodynamic processes in the greater Yellowstone region, western North America. *Geosphere*, *3*(4), 272–281. https://doi.org/10.1130/GES00083.1

Wittig, N., Pearson, D. G., Baker, J. A., Duggen, S., & Hoernle, K. (2010). A major element, PGE and Re–Os isotope study of middle Atlas (Morocco) peridotite xenoliths: Evidence for coupled introduction of metasomatic sulphides and clinopyroxene. *Lithos*, *115*(1–4), 15–26. https://doi.org/10.1016/j.lithos.2009.11.003

Wittig, N., Pearson, D. G., Duggen, S., Baker, J. A., & Hoernle, K. (2010). Tracing the metasomatic and magmatic evolution of continental mantle roots with Sr, Nd, Hf and and Pb isotopes: A case study of middle Atlas (Morocco) peridotite xenoliths. *Geochimica et Cosmochimica Acta*, *74*(4), 1417–1435. https://doi.org/10.1016/j.gca.2009.10.048

Wolff, J. A., Grandy, J. S., & Larson, P. B. (2000). Interaction of mantle-derived magma with island crust? Trace element and oxygen isotope data from the Diego Hernandez formation, Las Cañadas, Tenerife. *Journal of Volcanology and Geothermal Research*, *103*(1–4), 343–366. https://doi.org/10.1016/s0377-0273(00)00230-4

Wyllie, P. J., & Huang, W.-L. (1976). Carbonation and melting reactions in the system CaO–MgO–SiO_2–CO_2 at mantle pressures with geophysical and petrological applications. *Contributions to Mineralogy and Petrology*, *54*(2), 79–107. https://doi.org/10.1007/bf00372117

Zeyen, H., Ayarza, P., Fernàndez, M., & Rimi, A. (2005). Lithospheric structure under the western African-European plate boundary: A transect across the Atlas mountains and the Gulf of Cadiz. *Tectonics*, *24*(2), 1–16. https://doi.org/10.1029/2004TC001639

Zindler, A., & Hart, S. (1986). Chemical geodynamics. *Annual Review of Earth and Planetary Sciences*, *14*(1), 493–571. https://doi.org/10.1146/annurev.ea.14.050186.002425

15252027, 2023, 6, Downloaded from https://agupubs.onlinelibrary.wiley.com/doi/10.1029/2022GC010843 by Thorsten Becker - University Of Texas Libraries , Wiley Online Library on [12/06/2023]. See the Terms and Conditions (https://onlinelibrary.wiley.com/terms-and-conditions) on Wiley Online Library for rules of use; OA articles are governed by the applicable Creative Commons License